

# **The 2019 Raikoke eruption as a testbed for rapid assessment of volcanic atmospheric impacts by the Volcano Response group**

Jean-Paul Vernier<sup>1,2</sup>, Thomas J. Aubry<sup>3</sup>, Claudia Timmreck<sup>4</sup>, Anja Schmidt<sup>5,5b,5c</sup>, Lieven Clarisse<sup>6</sup>, Fred Prata<sup>7</sup>, Nicolas Theys<sup>8</sup>, Andrew T. Prata<sup>9,\*</sup>, Graham Mann<sup>10</sup>, Hyundeok Choi<sup>11</sup>, Simon Carn<sup>12</sup>, Richard Rigby<sup>13</sup>, Susan C. Loughlin<sup>14</sup> and John A. Stevenson<sup>14</sup>

(1) National Institute of Aerospace, Hampton, VA 23692

(2) NASA Langley Research Center, Hampton, VA 23692

(3) Department of Earth and Environmental Sciences, University of Exeter, Penryn, UK

(4) Max-Planck-Institut für Meteorologie, Hamburg, Germany

(5) Institute of Atmospheric Physics (IPA), German Aerospace Center (DLR), Oberpfaffenhofen, German

(5b) Meteorological Institute, Ludwig Maximilian University of Munich, Munich, Germany

(5c) Department of Chemistry, University of Cambridge, Cambridge, United Kingdom

(6) Université libre de Bruxelles (ULB), Service de Chimie Quantique et Photophysique, Atmospheric Spectroscopy, Brussels, Belgium

(7) AIRES Pty Ltd, Mt Eliza, Victoria, Australia

(8) Royal Belgian Institute for Space Aeronomy (BIRA-IASB), Brussels, Belgium

(9) Sub-Department of Atmospheric, Oceanic and Planetary Physics, University of Oxford, Oxford OX1 3PU, UK.

\*now at School of Earth, Atmosphere and Environment, Monash University, Clayton, Victoria 3800, Australia.

(10) University of Leeds, Leeds, UK.

(11) Science Applications International Corporation (SAIC), Inc. at NOAA/NWS/NCEP/Environmental Modeling Center, College Park, MD 20740

(12) Michigan Tech, USA

(13) Centre for Environmental Modelling and Computation, School of Earth and Environment, University of Leeds, UK

(14) British Geological Survey, Edinburgh, UK

*Correspondence to: Jean-Paul Vernier (jeanpaul.vernier@gmail.com)*

33 **Abstract.** The 21<sup>st</sup> June 2019 Raikoke eruption (48°N,153°E) generated one of the largest amounts of sulfur emission  
34 to the stratosphere since the 1991 Mt Pinatubo eruption. Satellite measurements indicate a consensus best estimate of  
35 1.5 Tg for the sulfur dioxide (SO<sub>2</sub>) injected at an altitude of around 14-15 km. The peak northern hemisphere mean  
36 525nm Stratospheric Aerosol Optical Depth (SAOD) increased to 0.025, a factor of three higher than background  
37 levels. The Volcano Response (VolRes) initiative provided a platform for the community to share information about  
38 this eruption, which significantly enhanced coordination efforts in the days after the eruption. A multi-platform  
39 satellite observation sub-group formed to prepare an initial report to present eruption parameters including SO<sub>2</sub>  
40 emissions and their vertical distribution for the modelling community. It allowed to make the first estimate of what  
41 would be the peak in SAOD one week after the eruption using a simple volcanic aerosol model. In this retrospective  
42 analysis, we show that revised volcanic SO<sub>2</sub> injection profiles yield a higher peak injection of the SO<sub>2</sub> mass. This  
43 highlights difficulties in accurately representing the vertical distribution for moderate SO<sub>2</sub> explosive eruptions in the  
44 lowermost stratosphere due to limited vertical sensitivity of current satellite sensors (+/- 2 km accuracy) and low  
45 horizontal resolution of lidar observations. We also show that the SO<sub>2</sub> lifetime initially assumed in the simple aerosol  
46 model was overestimated by 66%, pointing to challenges for simple models to capture how the life cycle of volcanic  
47 gases and aerosols depends on the SO<sub>2</sub> injection magnitude, latitude and height. Using revised injection profile,  
48 modelling results indicate a peak northern hemisphere monthly mean SAOD at 525nm of 0.024, in excellent agreement  
49 with observations, associated with a global monthly mean radiative forcing of -0.17 W/m<sup>2</sup> resulting in an annual global  
50 mean surface temperature anomalies of -0.028 K. Given the relatively small magnitude of the forcing, it is unlikely  
51 that the surface response can be dissociated from surface temperature variability.

## 52 **1. Introduction.**

53 After 95 years of dormancy, the Raikoke volcano in the Kuril Islands (North-West Pacific; 48.292°N, 153.25°E)  
54 began a series of explosions at 18UTC on 21 June 2019 lasting around 24 hours. Raikoke forms a small uninhabited  
55 Island of 2 km x 2.5 km which belongs to the Russian federation, 16 km from Matua Island in the Sea of Okhotsk.  
56 Its name originates from the ancient Japanese Ainu language and translate to “hellmouth”, referring to past volcanic  
57 eruptions. The first eruption reports of Raikoke originated from the mid-18<sup>th</sup> century but it was during the 1788  
58 eruption that one third of the Island was destroyed (Gorshkov, 1970). The last known eruption was reported in  
59 February 1924. Since then, the volcano remained dormant. The volcano is monitored by the Sakhalin Volcanic  
60 Eruption Response Team (SVERT), part of the Institute of marine geology and the Kamchatka Volcanic Eruption  
61 Response Team (KVERT). During the latest 2019 eruption, the first explosion of a series of 8 was reported by  
62 KVERT on 21 June at 17h50 UTC and quickly followed 1h later by a volcanic ash advisory produced by the Tokyo  
63 Volcanic Ash Advisory Center (VAAC) responsible to provide ash warnings to the International Civil Aviation  
64 Organization (ICAO) across the Pacific Northwest (Sennert, 2019). In addition, KVERT which issue volcano  
65 observatory notice warning for aviation had flagged with an aviation color code red which signifies that an “eruption  
66 was underway with significant emission ash into the atmosphere” (see KVERT webpage for more information  
67 <http://www.kscnet.ru/ivs/kvert/van/index?type=1>) . As a result, nearly 40 flights were re-routed to avoid volcanic  
68 ash clouds.

69 Firstov et al., (2020) analyzed Infrasound Signal (IS) from overpressure measurements from ground stations in  
70 Kamchatka and found a total of 12 explosive episodes (see Fig.1b). The first 8 episodes were followed by a  
71 continuous episode (9) which lasted for 3.5 h. Based on IS analysis, episodes are separated into magma  
72 fragmentation/ non-stationary processes and vent outflow (1,2,3,7,9 and 10) of ash-gas into the atmosphere. They  
73 were used to derive a minimal eruption tephra volume of 0.1 km<sup>3</sup> allowing to categorize the eruption as Volcanic  
74 Explosivity Index (VEI) 4 (Firstov et al., 2020). Fig.1a shows cloud top temperature (11µm) and associated cloud top  
75 heights derived from Himawari-8 geostationary satellite compared with IS data shown in Fig.1b. The eruption  
76 started at around 18:00 UTC on 21 June 2019 followed by at least 8 discrete “bursts” (eruptions) and continuous  
77 emissions. A further two discrete pulses occurred later. The IS analysis coincides very well with the Himawari-8  
78 observations where each IS corresponds to the release of volcanic cloud into the atmosphere. Muser et al. (2020)  
79 used one-dimensional volcanic plume models (Mastin, 2007; Folch et al., 2016) to invert the mass eruption rate of  
80 ash and initialize the ICON-ART (Zängl et al., 2015) dispersion model to investigate the complex aerosol,  
81 dynamical and radiative processes governing the plume evolution. More simplistic initialization approach with the  
82 dispersion model NAME (Beckett et al., 2020) and the aerosol-chemistry-climate model WACCM (Mills et al.,  
83 2016) were performed during the VolRes activities shortly after the eruption to assess the early dispersion of the  
84 plume.

85 As part of the scientific response to the eruption, the Volcano Response (Volres) initiative triggered an initial  
86 dialogue among the science community. VolRes is an international working group, within the Stratospheric Sulfur  
87 and its Role in Climate (SSiRC), to establish co-operation and community planning, for the next large-magnitude  
88 eruption, aligned also to the NASA initiative for US-based volcano response plan (Carn et al., 2021). The SSiRC  
89 initiative is itself an activity within the SPARC project of the World Climate Research Program (WCRP). Since its  
90 inception in 2015, VolRes consist of more than 250 scientists worldwide, from a diverse range of both model and  
91 observational experts, aiming to contribute from sharing and discussion of information related to the atmospheric  
92 impacts of volcanoes. Discussion and sharing to the mailing list is maintained through an archive and Wiki page,  
93 structured by eruption since 2018 (<https://wiki.earthdata.nasa.gov/display/volres>).

94 The discussions on the VolRes forum have mostly been focused towards: i) establishing initial estimates of the  
95 emitted SO<sub>2</sub> and ash, and injection heights estimates from multiple satellite observation platforms; ii) the expected  
96 impacts on stratospheric aerosol loadings; iii) factors to consider in modelling the aerosol cloud, towards then  
97 projecting radiative and climate effects; and iv) common related findings after other similar eruptions. Several cross-  
98 institutional co-operations resulted from the VolRes activity, which also motivated the Raikoke ACP/AMT/GMD  
99 inter-journal special issue “Satellite observations, in situ measurements and model simulations of the 2019 Raikoke  
100 eruption “. The Raikoke special issue includes a series of publications (Muser et al., 2020; Kloss et al., 2021;  
101 Vaughan et al., 2021; de Leeuw et al., 2021; Horváth et al., 2021a,b; Gorkavyi et al., 2021; Inness et al., 2022;  
102 Mingari et al., 2022; Osborne et al., 2022; Bruckert et al., 2022; Capponi et al., 2022; Cai et al., 2022; Harvey et al.,  
103 2022; Knepp et al., 2022; Prata et al., 2022; Petracca et al., 2022) focusing on the atmospheric impacts of this

104 eruption using satellite Low Earth Orbiting/Geostationary nadir and limb observations from UV-Visible to far IR,  
105 model simulations, airborne measurements and ground-based lidar observations.

106 The goals of this paper is to:

- 107 • Describe the activities undertaken by the Volcano Response group (VolRes,  
108 <https://wiki.earthdata.nasa.gov/display/volres>) at the time of the 2019 Raikoke eruption. A chronology of these  
109 activities is provided in Table 1.
- 110 • Give an overview of the early estimates of the mass of SO<sub>2</sub> emitted as well as the associated radiative forcing  
111 and temperature response inferred quickly after the eruption.
- 112 • Discuss how revised estimates of SO<sub>2</sub> mass and plume heights as well as radiative forcing estimates differ from  
113 the rapid assessment made a week after the eruption.
- 114 • Summarize the findings of the Raikoke special issue and highlight the remaining science questions as well as  
115 the challenges associated with rapid response to volcanic eruptions in the context of atmospheric impacts.

## 116 **2. Satellite Datasets**

### 117 **Himawari-8**

118 Himwari-8 is a spacecraft developed and operated by the Japanese Meteorological Organization (JAXA). The  
119 primary instrument aboard Himawari 8 is the Advanced Himawari Imager (AHI), a 16 multi-channel spectral  
120 imager to capture visible light and infrared images of the Asia-Pacific region at 500m horizontal resolution and  
121 every 10 minutes. AHI is used to derived the cloud-top temperature and associated cloud top height associated with  
122 the Raikoke eruption.

### 123 **TROPOMI**

124 The TROPospheric Monitoring Instrument (TROPOMI), onboard the Sentinel-5 Precursor satellite, provides  
125 atmospheric composition measurements (Veefkind et al., 2012) at high spatial resolution of 3.5 x 5.5 km<sup>2</sup>.  
126 TROPOMI is a hyperspectral sounder with different spectral bands from the ultraviolet (UV) to the short-wave  
127 infrared. TROPOMI provides nearly global coverage in one day at 1.30 pm local time. For a rapid assessment of the  
128 total emitted SO<sub>2</sub> mass, the operational SO<sub>2</sub> product (Theys et al., 2017) was used. A refined analysis was then  
129 performed with the scientific SO<sub>2</sub> layer height and vertical column joint retrieval of Theys et al.(2022)

### 130 **IASI**

131 The Infrared Atmospheric Sounding Interferometer (IASI) is the high spectral resolution infrared sounder onboard  
132 the operational Metop A-B-C platforms. With a morning and evening overpass (around 9:30 AM and PM),  
133 combined with a large swath, the instrument samples the entire globe twice a day. Its footprint is a 12km diameter  
134 circle at nadir viewing angles, gradually increasing to a 20 km x 39 km ellipse at the far end of its swath. The SO<sub>2</sub>  
135 product that was used for rapid assessment is the one detailed in Clarisse et al. (2014). The retrieval algorithm  
136 consists of two steps. First a so-called Z function that is estimated for each observed spectrum, using a set of

137 derivatives (Jacobians) with respect to the SO<sub>2</sub> partial columns at varying altitudes. The altitude at which Z function  
138 reaches is maximum is the retrieved SO<sub>2</sub> height. In a second step, the estimated SO<sub>2</sub> height is used to constrain the  
139 IASI SO<sub>2</sub> column retrieval. Note that the entire retrieval uses the 7.3 μm absorption band of SO<sub>2</sub>, which is less  
140 affected by ash than the 8.6 μm band. While the altitude algorithm has a general accuracy better than 2 km, it is  
141 known to underestimate the SO<sub>2</sub> altitude for high SO<sub>2</sub> columns. For the refined analysis discussed below, a new  
142 experimental product was used that deals better with saturation issues.

### 143 **Aqua/AIRS**

144 The atmospheric Infrared Radiation Sounder (AIRS) instrument is onboard the NASA polar-orbiting Aqua satellite  
145 at an altitude of about 705 km above the Earth surface with an equatorial crossing time at 1.30am/pm local time  
146 (Chahine et al., 2005; Prata & Bernardo, 2007). AIRS provides nearly continuous measurement coverage during  
147 14.5 orbits per day and a 95% global daily coverage with a swath of 1650 km and special resolution of 13.5 km x  
148 13.5 km at nadir (Tournigand et al., 2020). We use the version 7.0 AIRS level 2 Support Retrieval product, and the  
149 results are averaged into 1° x 1° grid cells in this analysis. The Brightness Temperature Difference (BTD, less than -  
150 6 K) is used as a proxy of SO<sub>2</sub> released from volcanoes. For more information about the AIRS BTD, see  
151 [https://docsserver.gesdisc.eosdis.nasa.gov/public/project/AIRS/V7\\_L2\\_Product\\_User\\_Guide.pdf](https://docsserver.gesdisc.eosdis.nasa.gov/public/project/AIRS/V7_L2_Product_User_Guide.pdf) (p102-103).

### 152 **CALIPSO/CALIOP**

153 The Cloud-Aerosol Lidar with Orthogonal Polarization (CALIOP), onboard the Cloud-Aerosol Lidar and Infrared  
154 Pathfinder Satellite Observations (CALIPSO) platform, has been providing aerosol vertical profile measurements of  
155 the Earth's atmosphere on a global scale since June 2006 (Winker et al., 2010). We use the version 4.21 CALIOP  
156 level 2 Aerosol layer and Cloud layer products, and only quality screened samples are used in the analysis. The  
157 Cloud Aerosol Discrimination (CAD) is the algorithm that evaluates CALIOP observables to classify layers and  
158 assign values between -100 (certainly aerosol) and 100 (certainly cloud). Aerosol layers with CAD score between -  
159 100 and -20 are selected to avoid low confidence (Winker et al., 2013; Tackett et al., 2018). Aerosol layers with the  
160 extinction Quality Control (QC) flag that are not equal to 0, 1, 16, and 18 are rejected to remove low confidence  
161 extinction retrievals. Detailed information of the QC flag can be found in Tackett et al. (2018). In addition, aerosol  
162 extinction samples with the extinction uncertainty equal to 99.99 km<sup>-1</sup> and all samples at lower altitudes in the  
163 profile are rejected to remove unreliable extinctions (Winker et al., 2013).

164

### 165 **3. Early reports of injection parameters one week after the eruption**

166 One of the main activities of a satellite subgroup formed within the framework of VolRes was to derive eruption  
167 parameters characterizing SO<sub>2</sub> emissions (e.g. mass, bulk height, injection profiles) as soon as possible so that  
168 modelers would run numerical simulations to understand the potential hazards and climate impacts of this eruption.  
169 The basic approach to estimate the total mass of SO<sub>2</sub> is similar for each satellite-based sensor. First, the process  
170 involves retrieving the Vertical Column Density (VDC, measured in molecules cm<sup>-2</sup> or g m<sup>-2</sup> or Dobson units) in

171 each pixel affected by SO<sub>2</sub>, followed by multiplying by the area of the pixels and integrating all the pixels to  
172 calculate the total SO<sub>2</sub> loadings. However, there are limitations to this method. Indeed, narrow swath width sensors,  
173 timing of the polar orbit and, in the case of the geostationary sensors, extreme viewing geometry (high satellite  
174 zenith angles) and movement out of the field of view will introduce errors (likely underestimations) of the total  
175 mass. There are also many assumptions used by the various algorithms that if not valid will introduce errors, as will  
176 be discussed hereunder. When the Vertical Column Densities (VCDs) are large (>500 DU) most algorithms have  
177 difficulty estimating the VCD correctly (Hyman and Pavolonis, 2020; Prata et al. 2021).

178 Figure 2 shows the time evolution of the total SO<sub>2</sub> mass during and after the Raikoke eruption from multiple  
179 sensors. The measurements discussed here all assume SO<sub>2</sub> in the UTLS (7–12 km). The SO<sub>2</sub> retrieved from  
180 Himawari-8 peaks near 1.5 Tg nearly 48h after the beginning of the eruption and follow similar temporal evolution  
181 as the one derived from Low Earth Orbit (LEO) satellites . Given the likelihood that most satellites underestimated  
182 the SO<sub>2</sub> mass, we chose at that time the maximum value from Himawari and the upper limits of the other sensors  
183 yielding a 1.5+/-0.2 Tg estimation. IASI, TROPOMI and CALIPSO data suggested that SO<sub>2</sub> was injected within a  
184 large altitude range from the ground up to well in the stratosphere (at least 15 km). In addition to a total mass of SO<sub>2</sub>  
185 (of 1.5 Tg), the VolRes team also issued a provisional vertical distribution of the emitted SO<sub>2</sub> mass that could be  
186 used by dispersion and climate modelers. To do so, IASI SO<sub>2</sub> height measurements on the 22<sup>nd</sup> June 2019 were used.  
187 The mass-altitude indicated that most SO<sub>2</sub> was released between 8-12 km with a secondary peak around 14-15 km.  
188 Scaled to the proposed 1.5 Tg, the distribution is shown in Figure 3 and is referred to as the ‘VolRes profile’ (blue  
189 line; also see Table 2). For TROPOMI, and other LEOs, the plume can be partly covered by a given orbit but using  
190 the multiple orbits of one day and the fact that they generally overlap most of the plume is covered. To avoid double  
191 counting, the data of one full day are usually averaged on a regular latitude-longitude grid, before the actual emitted  
192 SO<sub>2</sub> mass is calculated. An important source of error is the vertical distribution of SO<sub>2</sub>. In Fig.2, the retrieved SO<sub>2</sub>  
193 mass from TROPOMI was calculated by assuming a bulk plume height of 15 km (all plume heights given above sea  
194 level unless specified). This assumption can introduce errors (underestimation) in particular for clear-sky scenes and  
195 if the SO<sub>2</sub> is in the (lower) troposphere, typically below 7km, see e.g., Fig 1 of Theys et al. (2013). TROPOMI has  
196 less limitations in retrieving very large SO<sub>2</sub> columns (>500 DU) because in that case the spectral range used (360-  
197 390nm) is weakly affected by saturation due to non-linear SO<sub>2</sub> absorption (Bobrowski et al., 2010). The main  
198 problem is the presence of aerosols which are not explicitly treated in the retrievals (Theys et al., 2017). For ash, the  
199 photons cannot penetrate deep in the volcanic cloud (only the cloud top layer is sensed) and this leads to a strong  
200 underestimation of the mass of SO<sub>2</sub> (by a factor of 5 or so).

#### 201 **4. Revision and improvements of injection parameters.**

202 While the accuracy of the IASI SO<sub>2</sub> height retrievals is typically better than 2km, it became clear however that the  
203 VolRes profile was peaking too low in the atmosphere (e.g., de Leeuw et al., 2021). The main reason for this is related  
204 to the SO<sub>2</sub> Jacobians used in the retrieval. These are precalculated for relatively low SO<sub>2</sub> VCDs and are not directly  
205 applicable to saturated plumes, as encountered during the Raikoke eruption. Refinement of the IASI algorithm to  
206 better account for this dependence on the SO<sub>2</sub> loadings has led to SO<sub>2</sub> injection profile with a maximum SO<sub>2</sub> peaking

207 at ~14-15 km (see Figure 3) and a slightly lower total mass of ~1.3 Tg SO<sub>2</sub> (even though total mass estimates for the  
208 days after reach again 1.5 Tg and higher).

209 As an alternative to IASI, ultraviolet observations from the TROPOMI nadir sensor have been used to estimate the  
210 SO<sub>2</sub> injection profile (Table 2). Conceptually, the retrieval algorithm is like the IASI scheme. It relies on an iterative  
211 approach making use of a SO<sub>2</sub> optical depth look-up-table, where both SO<sub>2</sub> height and vertical column are retrieved  
212 jointly (Theys et al., 2021). The accuracy of the retrieved SO<sub>2</sub> heights is of 1-2 km, except when coincident with fresh  
213 and optically thick ash plumes for which the estimated heights can be strongly biased low. Because of this, the first  
214 reliable profile from TROPOMI which covers the full plume, is for the 24 June 2019. The maximum SO<sub>2</sub> height is  
215 found at ~11-12 km (Figure 3) and the total mass derived is of ~1.2 Tg SO<sub>2</sub>. However, the total mass is likely  
216 underestimated because only the pixels with confident SO<sub>2</sub> height retrievals are considered (typically for SO<sub>2</sub> columns  
217 > 5DU). Selected examples of retrieved SO<sub>2</sub> heights from the two instruments are illustrated in Figure 4.

218 Although the estimated SO<sub>2</sub> mass from IASI and TROPOMI agree well, the estimated SO<sub>2</sub> profiles show rather  
219 inconsistent results with a discrepancy of about 3km for the SO<sub>2</sub> center of mass. It should be emphasized that SO<sub>2</sub>  
220 height retrieval from nadir sensors is challenging in general but for Raikoke in particular. The retrievals and their  
221 interpretation might also suffer from different aspects. For instance, the UTLS was characterized by isothermal  
222 temperature profiles, which can lead to errors on the IASI height estimates. In addition, the measurement sensitivity  
223 is different in the ultraviolet than in the thermal infrared and depends on the way the photons interact with the volcanic  
224 cloud (and the constituents other than SO<sub>2</sub>). In this respect, the retrieved SO<sub>2</sub> heights must be considered as effective  
225 heights. Moreover, few CALIOP observations were available (see Section 6) for evaluating the results for the early  
226 stage of the eruption.

227 Despite these challenges, our injection profiles estimates are not in contradiction with results found in the literature:

- 228 • Kloss et al. (2021) reported a 14 km altitude plume height based on an early OMPS aerosol extinction profile,  
229 on 22 June 2019.
- 230 • Muser et al. (2020) derived typical altitudes of 8-14 km from MODIS and VIIRS cloud top height retrievals.
- 231 • By slightly adapting (assuming higher injection heights) the VolRes profile, de Leeuw et al. (2021) found  
232 the best match between modeled and TROPOMI SO<sub>2</sub> columns for an injection profile with most of SO<sub>2</sub>  
233 between 11 and 14 km.
- 234 • Hedelt et al. (2019) reported SO<sub>2</sub> heights similar to the TROPOMI results shown here, i.e., with the bulk  
235 height below 13km.
- 236 • SO<sub>2</sub> height retrievals from the Cross-track Infrared Sounder (CrIS) instrument (Hyman & Pavolonis, 2020)  
237 are consistent with plume heights as high as 14-17 km in the plume center, but also show that most of the  
238 SO<sub>2</sub> mass was emitted under 13 km.
- 239 • Geometric estimation of Raikoke ash column height suggests injection mainly between 5 and 14 km and an  
240 overshooting cloud up to 17 km (Horváth et al., 2021b).

- 241 • MLS data for 23-27 June indicates SO<sub>2</sub> plumes at 11 to 18 km with maximum columns observed around 14  
242 km (Gorkavyi et al., 2021).
- 243 • Using a Lagrangian transport model combined with TROPOMI and AIRS, Cai et al. (2022) reconstruct an  
244 emission profile with a peak at 11 km with a large spread from 6 to 14 km.
- 245 • Prata et al. (2022) found ash clouds at a maximum height of 14.2 km (median height of  $10.7 \pm 1.2$  km) during  
246 the main explosive phase.

## 247 **5. New plume injection analysis derived from CALIPSO and AIRS**

248 CALIPSO observations were made publicly available within 24-48 h after the beginning of the eruption, allowing  
249 accurate early estimates of the height of downwind plume sections. However, due to the narrow swath of the lidar (a  
250 few hundred meters) and consequently low spatial coverage, they may not completely represent the entire plume  
251 vertical distribution. Nevertheless, an overpass of the CALIPSO lidar across the plume on 22 June 2019 at 2.15 am,  
252 ~600 km east from the volcano within an SO<sub>2</sub> cloud observed by OMPS show volcanic layers between 9-13.5 km  
253 (Prata et al., 2021). A second overpass the next day depicts another volcanic layer between 15-16 km. Those  
254 observations were used to validate SO<sub>2</sub> emission profiles provided to the community a week after the eruption. Here,  
255 we give a more comprehensive analysis of the plume injection height using a combination of quasi-located (less  
256 than 1h apart) SO<sub>2</sub> observations from AIRS and detected volcanic layers from CALIOP during the first two weeks  
257 after the eruption. The brightness temperature difference ( $1361.44-1433.06 \text{ cm}^{-1}$ ) is used as a proxy of SO<sub>2</sub> released  
258 from volcanoes to identify CALIOP data within the SO<sub>2</sub> plume.

259 We combined SO<sub>2</sub> information from AIRS quasi-located observations from CALIOP to further investigate plume  
260 injection heights after the Raikoke eruption assuming that SO<sub>2</sub> and volcanic aerosols remained collocated in space  
261 and time during the first 10 days after the eruption. Figure 5a shows a map of SO<sub>2</sub> derived from AIRS together with  
262 CALIOP orbit tracks (red). The corresponding cloud and aerosol level 2 V4.2 products are plotted along with BT  
263 extracted along the orbit (Fig.5b). All corresponding layers (clouds and aerosols) associated with negative BT  
264 ( $\text{BTD} < 6 \text{ K}$ , red line Fig5c), indicating the presence of SO<sub>2</sub> in the atmospheric column, have been further analyzed to  
265 distinguish the volcanic plume. The distinction is based on the diagram of depolarization and color ratio shown in  
266 panel d. Figure 5a shows that CALIOP intersected the plume along two orbit tracks on 25 June. The first being  
267 along the 17h53 UTC orbit near 60°N and at two occasions between 55°N-65°N along the third orbit (from the left)  
268 near 14h36 UTC. The first intersection (numbered 1) shows the plume near 9-11 km with weak particulate  
269 DePolarization Ratio (DPR) ( $\text{DPR} < 0.2$ ) and particulate CoLor Ratio (CLR) near 0.5. DPR values suggest a mixture  
270 of ash and sulfate aerosols. However, the second set of intersections (numbered 2 and 3) of the plume shows higher  
271 DPR near 0.3 and the same CLR than the first indicating a higher fraction of ash particles resulting in increased DPR  
272 values. During those observations, two distinct plumes are visible, the northern intersection near 11-13 km (green  
273 color on diagrams) and a piece at higher altitude (13-15 km) further south ( $< 60^\circ\text{N}$ ).

274 We visually inspected all CALIOP observations (day and night) between 06/22 and 07/06 following the same  
275 approach and used plume identification criterion when  $\text{DPR} < 0.4$  and  $\text{CLR} < 0.7$  and altitude  $> 5$  km to remove  
276 tropospheric aerosols and ice clouds. Because of the enhanced noise of the daytime observations, we chose to focus



277 this analysis on nighttime data only. Figure 6 shows the daily observations of the Raikoke plume since the eruption  
278 and during the following two weeks. We note that the plume was observed by CALIOP from 8 km to 17 km. The  
279 cumulative Probability Density Function (pdf) suggests two main peaks, one near 10-11km km and another  
280 smoother peak near 13-15 km. The overall aerosol vertical distribution is consistent with the distribution of SO<sub>2</sub>  
281 profiles derived with different approaches and instruments just after the eruption (Fig.3). However, the pdf does not  
282 suggest a pronounced peak at a given altitude but rather a flatter distribution as opposed to what is shown in Figure  
283 3. The pdf does not account for or is not weighted by the aerosol loading, which may explain why we do not see a  
284 pronounced peak as for the SO<sub>2</sub> profiles derived from IASI and TROPOMI. In addition, SO<sub>2</sub> and volcanic aerosol  
285 layers are assumed to be collocated but it may not always be the case.

## 286 **6. Rapid projections of the aerosol forcing and the global mean surface temperature response.**

287 In the previous sections, we discussed in detail the methods used to derive injection parameters (SO<sub>2</sub> total mass,  
288 plume heights and SO<sub>2</sub> distribution) which served as input to estimate the radiative and surface temperature  
289 responses from the eruption in this section. Key metrics characterizing the climate effects of volcanic eruptions are  
290 the peak global mean mid-visible SAOD, the global mean net radiative forcing and the global mean surface  
291 temperature change. One motivation of the VolRes initiative is to provide an estimated magnitude for each of these  
292 metrics. In the case of a large-magnitude eruption, these initial indicators of the scale of the climate response would  
293 then help to determine whether resources should be directed towards additional measurement campaign and the  
294 forcing datasets enable the community to run seasonal and decadal forecasts.

295 The first estimates of the injected SO<sub>2</sub> mass and height became available 24-48 hours after the 2019 Raikoke  
296 eruption, followed one week later by an estimate of global mean peak SAOD (7.1), radiative forcing (7.2) and  
297 surface temperature (7.3). This section discusses: i) how these estimates were made; ii) how they compared to  
298 observations; and iii) ongoing improvements to the protocol for rapid projection of volcanic forcing and climate  
299 impact.

### 300 **6.1 Model simulations of aerosol optical properties**

301 We first made projections for SAOD on 25 June 2019 using EVA\_H (Aubry et al., 2020), a simple volcanic aerosol  
302 model based on inputs of the mass of volcanic SO<sub>2</sub> injected, its injection height, and the latitude of an eruption. The  
303 first estimates made following Raikoke used a range of injection heights between 10-20 km, and a range of the mass  
304 of SO<sub>2</sub> of 1-2 Tg of SO<sub>2</sub>, on the basis of first estimates of 14 km and 1.5 Tg of SO<sub>2</sub> that initially circulated on the  
305 VolRes mailing list (personal communication with Ghassan Taha and Lieven Clarisse). The corresponding  
306 simulated range in peak Northern Hemisphere (25°N-90°N, NH) monthly-mean SAOD at 525nm (SAOD<sub>525</sub>) was  
307 0.015-0.023 (Figure 7). This range was obtained using Monte Carlo methods, i.e. EVA\_H was run thousands of  
308 times, randomly resampling the range of injection height and mass. The negligible computational cost of simple  
309 models like EVA\_H is a key advantage for providing estimate of the volcanic SAOD perturbation and its  
310 uncertainties as soon as measurements of the SO<sub>2</sub> mass and its injection height become available. The SAOD  
311 perturbation was projected to be largely confined to 25-90°N (Figure 8). SAOD perturbations observed in the tropics

312 and Southern Hemisphere over 2019-2020 (Figure 8) are primarily driven by stratospheric emissions from the  
313 Ulawun 2019 eruptions and the Australian 2019-2020 wildfires (Kloss et al., 2021).

314 Following the communication of the initial VolRes SO<sub>2</sub> profile (Figure 3) through the VolRes mailing list, EVA\_H  
315 peak NH monthly-mean SAOD<sub>525</sub> estimate for Raikoke were revised to an even smaller value of 0.014. Compared to  
316 observations from GloSSAC (v2.1) (Kovilakam et al., 2020), this value was largely underestimated as GloSSAC NH  
317 monthly-mean SAOD<sub>525</sub> peaks at 0.025 (Figure 7, with GloSSAC in excellent agreement with observational values  
318 from Kloss et al., 2021) using OMPS-limb data. The new IASI June 22 profile presented in Figure 3 results in a  
319 higher peak NH monthly-mean SAOD<sub>525</sub> of 0.0175, with the higher proportion of stratospheric SO<sub>2</sub> in the new  
320 profile more than compensating for the total mass decreasing from 1.5 to 1.29 (average of the two IASI profiles) Tg  
321 of SO<sub>2</sub>. Although the new SO<sub>2</sub> emission profile improves agreement with observations, the estimated SAOD<sub>525</sub>  
322 value is still a substantial underestimate. Furthermore, the characteristic rise and decay timescales of the SAOD<sub>525</sub>  
323 perturbation are also overestimated by EVA\_H (Figure 7). These mismatches are caused by the constant timescale  
324 EVA\_H uses for SO<sub>2</sub> to sulfate aerosol conversion, which is biased towards an 8-month value adequate for the  
325 Pinatubo 1991 eruption (Aubry et al, 2020). If we decrease the value of this timescale by 66% to 2.8 month in  
326 EVA\_H, the NH peak SAOD value as well as the characteristic rise and decay timescale of the SAOD perturbation  
327 are in excellent agreement with observations for the 2019 Raikoke eruption (Figure 7). The fact that this model  
328 timescale is independent of the eruption characteristic is an already identified weakness of EVA\_H that will be  
329 addressed in future developments (Aubry et al., 2020). This timescale has indeed been shown to depend on the  
330 volcanic SO<sub>2</sub> mass (e.g. McKeen et al., 1984; Carn et al, 2016), injection altitude and latitude (e.g. Carn et al, 2016,  
331 Marshall et al. 2019) as well as co-emission of water vapor (Legrande et al., 2016) and volcanic ash (Zhu et al.,  
332 2022).

## 333 **6.2 Projection for global mean volcanic forcing**

334 On the same day that SAOD projections were initially provided, Piers Forster independently suggested via the  
335 VolRes mailing list (Forster, personal communication) that the global annual-mean net radiative forcing would be at  
336 most -0.2 W m<sup>-2</sup> (Figure 9, left) based on a scaling between the estimated SO<sub>2</sub> mass of 1.5 Tg SO<sub>2</sub> for 2019 Raikoke  
337 and the estimated 15-20 Tg SO<sub>2</sub> for the 1991 Mt. Pinatubo eruption, which resulted in a global annual-mean forcing  
338 of -3.2 W/m<sup>2</sup> in 1992. This projection was a back-of-the-envelope calculation using simple proportionality  
339 arguments and it did not rely on any SAOD estimates. A monthly global mean peak shortwave forcing with a range  
340 from -0.16 to -0.11 W/m<sup>2</sup> was derived from SAGE III observations (Kloss et al., 2021). The corresponding annual  
341 mean net forcing is expected to be much smaller because of the difference between the peak monthly NH mean  
342 SAOD and its average value over the first post-eruption year (Figure 7), as well as the fact that longwave  
343 stratospheric volcanic aerosol forcing can offset as much as half of the shortwave forcing (Schmidt et al. 2018).  
344 Altogether, the educated guess made for global annual mean radiative forcing was thus likely overestimated.

## 345 **6.3 Projection of the global mean surface temperature response**

346 Last, as part of the eruption response, one day after the first global annual-mean radiative forcing estimate of 0.2 W  
347 m<sup>-2</sup> was made using proportionality arguments and Pinatubo measurements (section 6.2 and Figure 9, left), we  
348 estimated that the peak global annual-mean surface temperature change would be -0.02 K (Figure 9, right). We  
349 obtained this estimate using FaIR, a simple climate model (Smith et al., 2018). Like EVA\_H, FaIR has a negligible  
350 computational cost enabling rapid estimates of global-mean surface temperature change following an eruption and  
351 facilitating uncertainty estimation, although the latter was not done for the 2019 Raikoke eruption. The model-  
352 projected surface temperature response cannot be compared to measurements owing to difficulties in disentangling  
353 such a small forced temperature response from temperature variations related to natural variability.

## 354 **7. Discussions**

355 The Raikoke eruption ended a period without moderate volcanic eruptions in the Northern Hemisphere since Nabro  
356 in 2011 (Bourassa et al., 2013, Fairlie et al., 2014; Sawamura et al., 2012) which injected 1.5-2 Tg of SO<sub>2</sub> partially  
357 distributed between the troposphere and stratosphere. Following the Nabro eruption, the role deep convection during  
358 the Summer Asian Monsoon was evoked to explain an apparent ascent of the plume (Bourassa et al., 2013) debated  
359 by others (Fromm et al., 2013, Vernier et al., 2013) based on initial observations of injection heights. The substantial  
360 debate provoked by this eruption clearly demonstrated the complexity of assessing accurately SO<sub>2</sub> injection heights  
361 and their partition relative to the tropopause. The VolRes initiative substantially helps fill those gaps by providing a  
362 coordinated structure to derive injection parameters after the Raikoke eruption. Multiple sensors were used to assess  
363 the total SO<sub>2</sub> mass and its distribution just one week after the eruption (Fig.3). However, the lack of vertically  
364 resolved SO<sub>2</sub> information remains a limitation to accurately assess SO<sub>2</sub> plume distribution and the revised estimates  
365 proposed here remain with a 2 km uncertainty regarding the exact position of the plume peak while the initial 1.5 Tg  
366 SO<sub>2</sub> mass estimate might be slightly overestimated. Advances in measuring SO<sub>2</sub> with lidar observations may fill  
367 those gaps in the future.

368 The VolRes team provided eruptive parameters within a week after the eruption that strongly helped modelers to  
369 estimate climate response of the Raikoke eruption. The use of simple models like EVA\_H and FaIR to project the  
370 climate response to an eruption in almost near real-time is a powerful way to generate first-order estimates of the  
371 perturbations to SAOD, and surface temperatures. Unlike simple proportionality arguments based on the Pinatubo  
372 1991 eruption, these models can estimate the time (and spatial, for EVA\_H) evolution of the response variable, and  
373 they account for complexities such as the dependency of SAOD on the SO<sub>2</sub> injection latitude and height. Their  
374 computationally inexpensive nature also enables a comprehensive quantification of uncertainties related to eruption  
375 source parameters, which are often poorly constrained in the days-months following an eruption as highlighted by  
376 this special issue, as well as uncertainties on parameters of these empirical models, such as the SO<sub>2</sub>-aerosol  
377 conversion timescale in EVA\_H (Figure 7).

378 One limitation of the application of these models following the Raikoke 2019 event is that they were not applied in  
379 concordance, i.e. FaIR was run using an expert guess for the radiative forcing instead of values derived from  
380 EVA\_H's SAOD estimates (see section 7.2 and 7.3). Following the Raikoke 2019 VolRes response, we combined  
381 the simple models EVA\_H (for aerosol forcing) and FaIR (for surface temperature response). To do so, we apply

382 simple linear (Schmidt et al., 2018) or exponential (Marshall et al., 2020) relationships to derive the global mean  
383 radiative forcing (FaIR's key input) from the global mean SAOD (one of EVA\_H's outputs). EVA\_H, SAOD-  
384 radiative forcing scalings, and FaIR were for example applied in concordance to estimate the climate impacts from  
385 the sulfate aerosols of the January 2022 Hunga Tonga-Hunga Ha'apai eruption. These models have been combined  
386 into a single dedicated webtool called Volc2Clim (Schmidt et al., 2023), publicly available at  
387 <https://volc2clim.bgs.ac.uk/>. Applied to Raikoke 2019 using the new injection profile (Figure 3) and revised SO<sub>2</sub> to  
388 sulfate aerosol conversion timescale, the beta version of Volc2Clim projected peak global mean of 0.008, -0.17  
389 W/m<sup>2</sup> and -0.028 K for monthly mean SAOD, monthly mean radiative forcing and annual mean temperature  
390 anomaly. In addition to key metrics discussed in this section such as global mean SAOD, radiative forcing and  
391 surface temperature, aerosol optical properties field (dependent on latitude, altitude and wavelength) are outputted  
392 by Volc2Clim for use in climate models that do not have an interactive stratospheric aerosol scheme. With a webtool  
393 for rapid estimation of the global climate response during an eruptive crisis, we hope to support communication  
394 amongst the scientific community (including VolRes), with authorities and with the public, which in turn will help  
395 to mitigate potential consequences arising from the climate effects of an eruption.

396 Although Volc2Clim offers new perspectives for rapid response and communication following volcanic eruptions,  
397 the simplified nature of the models at its core means their result should be considered carefully. As an example,  
398 EVA\_H currently directly scales the global mean aerosol effective radius from the total mass of aerosol (Aubry et  
399 al., 2020). Even for the 1991 Pinatubo eruption, the aerosol effective radius time evolution lagged that of the total  
400 mass (e.g. Toohey et al., 2016). Furthermore, Wrana et al. (2023) show that some eruptions injecting less than 1 Tg  
401 SO<sub>2</sub> into the stratosphere lead to a reduction of aerosol size, a response opposite to that predicted by EVA\_H and  
402 thus Volc2Clim. Beyond volcanic sulfate aerosol, Volc2Clim currently does not allow projections of effects related  
403 to co-emission of species such as water vapor or halogen in volcanic plumes, or PyroCumulonimbus (PyroCbs)  
404 plumes. Before and after the Raikoke eruption, three significant events affected stratospheric aerosols. Indeed, SO<sub>2</sub>  
405 injected from the June an August 2019 Ulawun eruptions and smoke from PyroCbs in Canada made the Raikoke  
406 eruption even more challenging to understand. The PyroCbs in Canada produced smoke in the UTLS one week  
407 before the eruption, but the transport patterns of smoke and volcanic aerosols have been distinct (Osborne et al.,  
408 2022) and the likelihood for both plumes to mix is relatively small. The Ulawun eruption injected SO<sub>2</sub> which  
409 remained relatively confined in the Southern Hemisphere, but we cannot rule out that both plumes got mixed in the  
410 tropics (Kloss et al., 2021). The relatively small amount of SO<sub>2</sub> injected by Ulawun (< 0.1 Tg) was not considered  
411 in the estimates provided in this paper. Another interesting feature observed after the Raikoke eruption was the  
412 formation of a distinct plume which rose into the stratosphere. The plume formed a vortex circulation which  
413 remained coherent for several weeks (Gorkavyi et al., 2021) rising in the stratosphere of 10 km over the course of 2-  
414 3 months. While this plume shared similar optical properties to smoke, Knepp et al. (2022) concluded that this layer  
415 was mostly composed of large sulfuric acid droplets but did not refute the possible presence of a fine ash  
416 component. More recently (Khaykin et al, 2023) found that 24% of the total SO<sub>2</sub> mass was contained in the volcanic  
417 vortex with a confined anticyclonic circulation detected by wind doppler lidar from Aeolus. A warm anomaly of 1 K  
418 was also evident GPS RO Cosmic data demonstrating that the heating of the plume was indeed responsible for its

419 internal circulation and maintenance. Moreover, the properties of the plume observed by CALIOP showed the  
420 persistence of ash that likely induced internal heating in the plume consistent with earlier observations of volcanic  
421 clouds after the Kelud and Puyehue-Cordon eruptions (Jensen et al., 2018; Vernier et al., 2013, 2016). While the  
422 presence of fine ash in the Raikoke could likely explained the maintenance of the vortex as observed after PyroCbs  
423 events but with a much faster ascent rate, the interplay between ash and sulfate and influence on radiative  
424 calculations is still not understood (Vernier et al., 2016; Stenchikov et al., 2021; Zhu et al., 2020). In addition, we  
425 cannot fully rule out that remnants of smoke from the PyroCbs in Canada one week before the eruption could have  
426 played a role in the transport of the plume. The increased lifetime of this plume may have produced a larger climate  
427 impact than expected since this effect is not included in the simple model provided in this paper (Figure 8). Besides,  
428 we cannot rule out that the lower plume lifetime maybe have been affected and influenced by wildfires from Siberia  
429 during the summer 2019 as suggested by Ohneiser et al. (2021).

430 Finally, the recent eruption of Hunga Tonga Hunga Ha’apai (HTHH) demonstrated that sub-marine eruption can  
431 inject significant amount of H<sub>2</sub>O in the stratosphere (Milan et al., 2022, Vogel et al., 2022; Sellitto et al., 2022)  
432 which is known to have opposite cooling climate effects than sulfate aerosol. The water vapor can reduce the  
433 lifetime of SO<sub>2</sub> by providing OH radicals and affect aerosol size distribution through condensational growth (Zhu et  
434 al., 2022). Such effects are not included in the simple climate estimates provided here and would limit its  
435 applicability in the case of HTHH if only the climate impacts of sulfate aerosols are considered.

## 436 **8. Conclusion**

437 VolRes is an international coordinated initiative to study the atmospheric impacts of volcanic eruptions, now  
438 involving more than 250 researchers worldwide. The 2019 Raikoke eruption triggered significant responses by the  
439 VolRes community through exchanges of information via the mailing list and the preparation of SO<sub>2</sub> profile  
440 recommendations for modelers made available a week after the eruption only. Our paper gives a brief overview of  
441 how the community responded to this volcanic eruption, which is documented extensively in the Raikoke special  
442 issue. We then described how early estimates of SO<sub>2</sub> emission and height, a fundamental parameter which dictates  
443 the plume lifetime and its impacts, were derived from satellite observations. These estimates were used by VolRes to  
444 calculate SAOD, radiative forcings and surface temperature changes as part of the initial eruption response. We  
445 revisited the initial SO<sub>2</sub> injection profiles by addressing saturation effects due to high SO<sub>2</sub> column density to  
446 improve plume injection heights. We highlight remaining challenges in accurately representing the vertical  
447 distribution for moderate- SO<sub>2</sub> explosive eruptions in the lowermost stratosphere due to limited vertical sensitivity of  
448 current satellite sensors (+/- 2 km accuracy) and low horizontal resolution of lidar observations. We found that using  
449 revisited SO<sub>2</sub> injection heights and reduced SO<sub>2</sub>-aerosol conversion timescale in a simple volcanic aerosol model  
450 (EVA\_H) improves SAOD estimates relative to available observations from the GloSSAC dataset. The protocol for  
451 fast estimation of aerosol optical properties, radiative forcing and surface temperature response to volcanic eruption  
452 has since been implemented in a seamless webtool (Volc2Clim, <https://volc2clim.bgs.ac.uk/>). The computationally  
453 inexpensive nature of the webtool makes it ideal for rapid assessment of the volcanic climate effect and for  
454 propagating large uncertainties that characterize early observations of volcanic clouds. Further development of the

455 underlying simple models as well as continued use of complex models explicitly modelling aerosol chemistry,  
456 microphysics and transport remain critical given the complex nature of volcanic events. For example, the Raikoke  
457 eruption took place in connection with two eruptions of Ulawun in June and August 2019 and just after a PyroCb  
458 event which transported smoke into the stratosphere which were not considered in our original or revised  
459 calculations. In addition, the recent HTHH eruption demonstrated that water vapor can also be injected into the  
460 stratosphere which can affect SO<sub>2</sub> and aerosol lifetime but also with a radiative forcing that is opposite to volcanic  
461 sulfate aerosols.

## 462 **Competing interests**

463 The contact author has declared that none of the authors has any competing interests.

## 464 **Acknowledgement.**

465 JPV and HC were supported by the NASA Roses program through the SAGE III Science Team (80NSSC21K1195)  
466 and Upper Atmosphere Composition Observations program (80NSSC21K1082). TJA was supported by a global  
467 mobility grant from the University of Exeter and a travel award from the Canada-UK foundation. CT acknowledges  
468 support for this research by the Deutsche Forschungsgemeinschaft Research Unit VolImpact (FOR2820,398006378)  
469 within the project VolClim (TI 344/2-1). ATP acknowledges funding from the Natural Environment Research  
470 Council (NERC) R4Ash project (NE/S003843/1). The Volc2Clim tool was kindly supported by the UK Earth  
471 System Modelling project, funded by the UKRI – Natural Environment Research Council (NERC) national  
472 capability grant number NE/N017951/1 and the Met Office, as well as NERC grants NE/S000887/1 (VOL-CLIM)  
473 and NE/S00436X/1 (V-PLUS). The GloSSAC data were obtained from the NASA Langley Research Center  
474 Atmospheric Sciences Data Center. The Volc2Clim webtool is available at <https://volc2clim.bgs.ac.uk/>, and the  
475 source code is available on GitHub at <https://github.com/cemac/volc2clim/>. The source code of the EVA\_H volcanic  
476 aerosol model is available on GitHub at [https://github.com/thomasaubry/EVA\\_H](https://github.com/thomasaubry/EVA_H). The source code of the FaIR  
477 climate model is available on Github at <https://github.com/OMS-NetZero/FAIR>.

478

## 479 **References:**

480  
481 Aubry, T. J., Toohey, M., Marshall, L., Schmidt, A., & Jellinek, A. M. (2020). A New Volcanic Stratospheric  
482 Sulfate Aerosol Forcing Emulator (EVA\_H): Comparison With Interactive Stratospheric Aerosol Models.  
483 *Journal of Geophysical Research: Atmospheres*, 125(3), e2019JD031303.  
484 <https://doi.org/https://doi.org/10.1029/2019JD031303>  
485

486 Beckett, Frances M., et al. "Atmospheric dispersion modelling at the London VAAC: A review of developments  
487 since the 2010 eyjafjallajökull volcano ash cloud." *Atmosphere* 11.4 (2020): 352.  
488

489 Bobrowski, N., Kern, C., Platt, U., Hörmann, C., & Wagner, T. (2010). Novel SO<sub>2</sub> spectral evaluation scheme using  
490 the 360–390 nm wavelength range. *Atmospheric Measurement Techniques*, 3(4), 879–891.  
491 <https://doi.org/10.5194/amt-3-879-2010>  
492

493 Bourassa, A. E., Robock, A., Randel, W. J., Deshler, T., Rieger, L. A., Lloyd, N. D., Llewellyn, E. J. (Ted), &  
494 Degenstein, D. A. (2012). Large Volcanic Aerosol Load in the Stratosphere Linked to Asian Monsoon  
495 Transport. *Science*, 337(6090), 78–81. <https://doi.org/10.1126/science.1219371>  
496

497 Bruckert, J., Hoshyaripour, G. A., Horváth, Á., Muser, L. O., Prata, F. J., Hoose, C., and Vogel, B.: Online treatment  
498 of eruption dynamics improves the volcanic ash and SO<sub>2</sub> dispersion forecast: case of the 2019 Raikoke  
499 eruption, *Atmos. Chem. Phys.*, 22, 3535–3552, <https://doi.org/10.5194/acp-22-3535-2022>, 2022.  
500

501 Cai, Z., Griessbach, S., & Hoffmann, L. (2022). Improved estimation of volcanic SO<sub>2</sub> injections from satellite  
502 retrievals and Lagrangian transport simulations: the 2019 Raikoke eruption. *Atmospheric Chemistry and*  
503 *Physics*, 22(10), 6787–6809. <https://doi.org/10.5194/acp-22-6787-2022>  
504

505 Capponi, A., Harvey, N. J., Dacre, H. F., Beven, K., Saint, C., Wells, C., and James, M. R.: Refining an ensemble of  
506 volcanic ash forecasts using satellite retrievals: Raikoke 2019, *Atmos. Chem. Phys.*, 22, 6115–6134,  
507 <https://doi.org/10.5194/acp-22-6115-2022>, 2022.  
508

509 Carn, S. A., Clarisse, L., & Prata, A. J. (2016). Multi-decadal satellite measurements of global volcanic degassing.  
510 *Journal of Volcanology and Geothermal Research*, 311, 99-134.  
511

512 Carn, S. A., Newman, P. A., Aquila, V., Gonnermann, H., & Dufek, J. (2021). Anticipating climate impacts of major  
513 volcanic eruptions. *Eos*, 102.  
514

515 Chahine, M., Barnet, C., Olsen, E. T., Chen, L., & Maddy, E. (2005). On the determination of atmospheric minor  
516 gases by the method of vanishing partial derivatives with application to CO<sub>2</sub>. *Geophysical Research*  
517 *Letters*, 32(22). <https://doi.org/https://doi.org/10.1029/2005GL024165>  
518

519 Clarisse, L., Coheur, P.-F., Theys, N., Hurtmans, D., and Clerbaux, C.: The 2011 Nabro eruption, a SO<sub>2</sub> plume  
520 height analysis using IASI measurements, *Atmos. Chem. Phys.*, 14, 3095–3111,  
521 <https://doi.org/10.5194/acp-14-3095-2014>, 2014.  
522

523 de Leeuw, J., Schmidt, A., Witham, C. S., Theys, N., Taylor, I. A., Grainger, R. G., Pope, R. J., Haywood, J.,  
524 Osborne, M., & Kristiansen, N. I. (2021). The 2019 Raikoke volcanic eruption -- Part 1: Dispersion model  
525 simulations and satellite retrievals of volcanic sulfur dioxide. *Atmospheric Chemistry and Physics*, 21(14),

526 10851–10879. <https://doi.org/10.5194/acp-21-10851-2021>  
527  
528 Fairlie, T. D., Vernier, J.-P., Natarajan, M., & Bedka, K. M. (2014). Dispersion of the Nabro volcanic plume and its  
529 relation to the Asian summer monsoon. *Atmospheric Chemistry and Physics*, 14(13).  
530 <https://doi.org/10.5194/acp-14-7045-2014>  
531  
532 Firstov, P. P., Popov, O. E., Lobacheva, M. A., Budilov, D. I., & Akbashev, R. R. (2020). *Wave perturbations in the*  
533 *atmosphere accompanied the eruption of the Raykoke volcano (Kuril Islands) 21--22 June, 2019.*  
534  
535 Folch, A., Costa, A., and Macedonio, G.: FPLUME-1.0: An integral volcanic plume model accounting for ash  
536 aggregation, *Geosci. Model. Dev.*, 9, 431–450, <https://doi.org/10.5194/gmd9-431-2016>, 2016.  
537  
538 Fromm, M., Nedoluha, G., & Charvát, Z. (2013). Comment on “Large Volcanic Aerosol Load in the Stratosphere  
539 Linked to Asian Monsoon Transport.” *Science*, 339(6120), 647. <https://doi.org/10.1126/science.1228605>  
540  
541 Hedelt, P., Efremenko, D. S., Loyola, D. G., Spurr, R., and Clarisse, L.: Sulfur dioxide layer height retrieval from  
542 Sentinel-5 Precursor/TROPOMI using FP\_ILM, *Atmos. Meas. Tech.*, 12, 5503–5517,  
<https://doi.org/10.5194/amt-12-5503-2019>, 2019  
543  
544 Gorkavyi, N., Krotkov, N., Li, C., Lait, L., Colarco, P., Carn, S., DeLand, M., Newman, P., Schoeberl, M., Taha, G.,  
545 Torres, O., Vasilkov, A., & Joiner, J. (2021). Tracking aerosols and SO<sub>2</sub> clouds from the Raikoke eruption:  
546 3D view from satellite observations. *Atmospheric Measurement Techniques*, 14(12), 7545–7563.  
<https://doi.org/10.5194/amt-14-7545-2021>  
547  
548 Gorshkov G S, 1970, *Volcanism and the Upper Mantle; Investigations in the Kurile Island Arc*, New York: Plenum  
549 Publishing Corp, 385 p.  
550  
551 Harvey, N. J., Dacre, H. F., Saint, C., Prata, A. T., Webster, H. N., and Grainger, R. G.: Quantifying the impact of  
552 meteorological uncertainty on emission estimates and the risk to aviation using source inversion for the  
553 Raikoke 2019 eruption, *Atmos. Chem. Phys.*, 22, 8529–8545, <https://doi.org/10.5194/acp-22-8529-2022>,  
554 2022.  
555  
556 Horváth, Á., Carr, J. L., Girina, O. A., Wu, D. L., Bril, A. A., Mazurov, A. A., Melnikov, D. V., Hoshyaripour, G.  
557 A., and Buehler, S. A.: Geometric estimation of volcanic eruption column height from GOES-R near-limb  
558 imagery – Part 1: Methodology, *Atmos. Chem. Phys.*, 21, 12189–12206, [https://doi.org/10.5194/acp-21-](https://doi.org/10.5194/acp-21-12189-2021)  
559 [12189-2021](https://doi.org/10.5194/acp-21-12189-2021), 2021a.

560  
561



562 Horváth, Á., Girina, O. A., Carr, J. L., Wu, D. L., Bril, A. A., Mazurov, A. A., Melnikov, D. V, Hoshyaripour, G.  
563 A., & Buehler, S. A. (2021). Geometric estimation of volcanic eruption column height from GOES-R near-  
564 limb imagery -- Part 2: Case studies. *Atmospheric Chemistry and Physics*, 21(16), 12207–12226.  
565 <https://doi.org/10.5194/acp-21-12207-2021b>  
566

567 Hyman, D. M. and Pavolonis, M. J.: Probabilistic retrieval of volcanic SO<sub>2</sub> layer height and partial column density  
568 using the Cross-track Infrared Sounder (CrIS), *Atmospheric Measurement Techniques*, 13, 5891–5921,  
569 <https://doi.org/10.5194/amt-13-5891-2020>, 2020.  
570  
571

572 Inness, A., Ades, M., Balis, D., Efremenko, D., Flemming, J., Hedelt, P., Koukouli, M.-E., Loyola, D., and Ribas,  
573 R.: Evaluating the assimilation of S5P/TROPOMI near real-time SO<sub>2</sub> columns and layer height data into  
574 the CAMS integrated forecasting system (CY47R1), based on a case study of the 2019 Raikoke eruption,  
575 *Geosci. Model Dev.*, 15, 971–994, <https://doi.org/10.5194/gmd-15-971-2022>, 2022.  
576

577 Jensen, E. J., Woods, S., Lawson, R. P., Bui, T. P., Pfister, L., Thornberry, T. D., Rollins, A. W., Vernier, J.-P., Pan,  
578 L. L., Honomichl, S., & Toon, O. B. (2018). Ash Particles Detected in the Tropical Lower Stratosphere.  
579 *Geophysical Research Letters*, 45(20). <https://doi.org/10.1029/2018GL079605>.  
580

581 Khaykin, S.M., de Laat, A.T.J., Godin-Beekmann, S. *et al.* Unexpected self-lofting and dynamical confinement of  
582 volcanic plumes: the Raikoke 2019 case. *Sci Rep* 12, 22409 (2022). [https://doi.org/10.1038/s41598-022-](https://doi.org/10.1038/s41598-022-27021-0)  
583 [27021-0](https://doi.org/10.1038/s41598-022-27021-0)  
584

585 Kloss, C., Berthet, G., Sellitto, P., Ploeger, F., Taha, G., Tidiga, M., Eremenko, M., Bossolasco, A., Jégou, F.,  
586 Renard, J.-B., & Legras, B. (2021). Stratospheric aerosol layer perturbation caused by the 2019 Raikoke  
587 and Ulawun eruptions and their radiative forcing. *Atmospheric Chemistry and Physics*, 21(1), 535–560.  
588 <https://doi.org/10.5194/acp-21-535-2021>  
589

590 Knepp, T. N., Thomason, L., Kovilakam, M., Tackett, J., Kar, J., Damadeo, R., and Flittner, D.: Identification of  
591 smoke and sulfuric acid aerosol in SAGE III/ISS extinction spectra, *Atmos. Meas. Tech.*, 15, 5235–5260,  
592 <https://doi.org/10.5194/amt-15-5235-2022>, 2022.  
593

594 Kovilakam, M., Thomason, L. W., Ernest, N., Rieger, L., Bourassa, A., & Millán, L. (2020). The Global Space-  
595 based Stratospheric Aerosol Climatology (version 2.0): 1979--2018. *Earth System Science Data*, 12(4),  
596 2607–2634. <https://doi.org/10.5194/essd-12-2607-2020>  
597

598 LeGrande, A., Tsigaridis, K. & Bauer, S. Role of atmospheric chemistry in the climate impacts of stratospheric

599 volcanic injections. *Nature Geosci* 9, 652–655 (2016). <https://doi.org/10.1038/ngeo2771>  
600

601 Marshall, L., Johnson, J. S., Mann, G. W., Lee, L., Dhomse, S. S., Regayre, L., et al. (2019). Exploring how eruption  
602 source parameters affect volcanic radiative forcing using statistical emulation. *Journal of Geophysical*  
603 *Research: Atmospheres*, 124, 964–985. <https://doi.org/10.1029/2018JD028675>  
604

605 Marshall, L. R., Smith, C. J., Forster, P. M., Aubry, T. J., Andrews, T., & Schmidt, A. (2020). Large variations in  
606 volcanic aerosol forcing efficiency due to eruption source parameters and rapid adjustments. *Geophysical*  
607 *Research Letters*, 47, e2020GL090241. <https://doi.org/10.1029/2020GL090241>  
608

609 Mastin, L. G.: A user-friendly one-dimensional model for wet volcanic plumes, *Geochem. Geophys. Geosy.*, 8,  
610 <https://doi.org/10.1029/2006GC001455>, 2007.  
611

612 McKeen, S.A., Liu, S.C. and Kiang, C.S., 1984. On the chemistry of stratospheric SO<sub>2</sub> from volcanic eruptions.  
613 *Journal of Geophysical Research: Atmospheres*, 89(D3), pp.4873-4881.  
614

615 Mills, M. J., et al. (2016), Global volcanic aerosol properties derived from emissions, 1990–2014, using  
616 CESM1(WACCM), *J. Geophys. Res. Atmos.*, 121, 2332–2348, doi:10.1002/2015JD024290.

617 Millán, L., Santee, M. L., Lambert, A., Livesey, N. J., Werner, F., Schwartz, M. J., et al. (2022). The Hunga Tonga-  
618 Hunga Ha'apai Hydration of the Stratosphere. *Geophysical Research Letters*, 49,  
619 e2022GL099381. <https://doi.org/10.1029/2022GL099381>

620 Mingari, L., Folch, A., Prata, A. T., Pardini, F., Macedonio, G., and Costa, A.: Data assimilation of volcanic aerosol  
621 observations using FALL3D+PDAF, *Atmos. Chem. Phys.*, 22, 1773–1792, [https://doi.org/10.5194/acp-22-](https://doi.org/10.5194/acp-22-1773-2022)  
622 [1773-2022](https://doi.org/10.5194/acp-22-1773-2022), 2022.  
623

624 Müller, W. A., Jungclaus, J. H., Mauritsen, T., Baehr, J., Bittner, M., Budich, R., et al. (2018). A higher-resolution  
625 version of the Max Planck Institute Earth System Model (MPI-ESM1.2-HR). *Journal of Advances in*  
626 *Modeling Earth Systems*, 10, 1383–1413. <https://doi.org/10.1029/2017MS001217>  
627

628

629 Muser, L. O., Hoshyaripour, G. A., Bruckert, J., Horváth, Á., Malinina, E., Wallis, S., Prata, F. J., Rozanov, A., von  
630 Savigny, C., Vogel, H., & Vogel, B. (2020). Particle aging and aerosol-radiation interaction affect volcanic  
631 plume dispersion: evidence from the Raikoke 2019 eruption. *Atmospheric Chemistry and Physics*, 20(23),  
632 15015–15036. <https://doi.org/10.5194/acp-20-15015-2020>  
633

634  
635 Ohneiser, K., Ansmann, A., Chudnovsky, A., Engelmann, R., Ritter, C., Veselovskii, I., Baars, H., Gebauer, H.,  
636 Griesche, H., Radenz, M., Hofer, J., Althausen, D., Dahlke, S., and Maturilli, M.: The unexpected smoke  
637 layer in the High Arctic winter stratosphere during MOSAiC 2019–2020, *Atmos. Chem. Phys.*, 21, 15783–  
638 15808, <https://doi.org/10.5194/acp-21-15783-2021>, 2021.

639  
640 Osborne, M. J., de Leeuw, J., Witham, C., Schmidt, A., Beckett, F., Kristiansen, N., Buxmann, J., Saint, C., Welton,  
641 E. J., Fochesatto, J., Gomes, A. R., Bundke, U., Petzold, A., Marenco, F., & Haywood, J. (2022). The 2019  
642 Raikoke volcanic eruption - Part 2: Particle-phase dispersion and concurrent wildfire smoke emissions.  
643 *Atmospheric Chemistry and Physics*, 22(5), 2975–2997. <https://doi.org/10.5194/acp-22-2975-2022>  
644

645 Petracca, I., De Santis, D., Picchiani, M., Corradini, S., Guerrieri, L., Prata, F., Merucci, L., Stelitano, D., Del Frate,  
646 F., Salvucci, G., and Schiavon, G.: Volcanic cloud detection using Sentinel-3 satellite data by means of  
647 neural networks: the Raikoke 2019 eruption test case, *Atmos. Meas. Tech.*, 15, 7195–7210,  
648 <https://doi.org/10.5194/amt-15-7195-2022>, 2022.

649  
650 Prata, A. J., & Bernardo, C. (2007). Retrieval of volcanic SO<sub>2</sub> column abundance from Atmospheric Infrared  
651 Sounder data. *Journal of Geophysical Research: Atmospheres*, 112(D20).  
652 <https://doi.org/https://doi.org/10.1029/2006JD007955>  
653

654 Prata, A. T., Mingari, L., Folch, A., Macedonio, G., and Costa, A.: FALL3D-8.0: a computational model for  
655 atmospheric transport and deposition of particles, aerosols and radionuclides – Part 2: Model validation,  
656 *Geosci. Model Dev.*, 14, 409–436, <https://doi.org/10.5194/gmd-14-409-2021>, 2021.

657  
658 Prata, A. T., Grainger, R. G., Taylor, I. A., Povey, A. C., Proud, S. R., and Poulsen, C. A.: Uncertainty-bounded  
659 estimates of ash cloud properties using the ORAC algorithm: application to the 2019 Raikoke eruption,  
660 *Atmos. Meas. Tech.*, 15, 5985–6010, <https://doi.org/10.5194/amt-15-5985-2022>, 2022.

661  
662 Sawamura, P., Vernier, J. P., Barnes, J. E., Berkoff, T. A., Welton, E. J., Alados-Arboledas, L., Navas-Guzmán, F.,  
663 Pappalardo, G., Mona, L., Madonna, F., Lange, D., Sicard, M., Godin-Beekmann, S., Payen, G., Wang, Z.,  
664 Hu, S., Tripathi, S. N., Cordoba-Jabonero, C., & Hoff, R. M. (2012). Stratospheric AOD after the 2011  
665 eruption of Nabro volcano measured by lidars over the Northern Hemisphere. *Environmental Research*  
666 *Letters*, 7(3). <https://doi.org/10.1088/1748-9326/7/3/034013>  
667

668 Sellitto, P., Podglajen, A., Belhadji, R., Boichu, M., Carboni, E., Cuesta, J., Duchamp, C., Kloss, C., Siddans, R.,  
669 Bègue, N., Blarel, L., Jegou, F., Khaykin, S., Renard, J.-B., & Legras, B. (2022). The unexpected radiative  
670 impact of the Hunga Tonga eruption of 15th January 2022. *Communications Earth & Environment*, 3(1), 288.

671 <https://doi.org/10.1038/s43247-022-00618-z>  
672  
673 Sennert, 2019. Global Volcanism Program, 2019. Report on Raikoke (Russia). Weekly Volcanic Activity Report, 26  
674 June-2 July 2019. Smithsonian Institution and US Geological Survey.

675 Schmidt, A., et al. (2018). Volcanic radiative forcing from 1979 to 2015. *Journal of Geophysical Research:*  
676 *Atmospheres*, 123(22), 12491-12508.  
677

678 Schmidt, A., Aubry, T.J., Rigby, R., Stevenson, J. and Loughlin, S., Volc2Clim online tool, 2023,  
679 <https://doi.org/10.5281/zenodo.7602062>, <https://volc2clim.bgs.ac.uk/>.

680

681 Smith, C. J., Forster, P. M., Allen, M., Leach, N., Millar, R. J., Passerello, G. A., & Regayre, L. A. (2018). FAIR  
682 v1.3: a simple emissions-based impulse response and carbon cycle model. *Geoscientific Model*  
683 *Development*, 11(6), 2273–2297. <https://doi.org/10.5194/gmd-11-2273-2018>  
684

685 Stenchikov, G., Ukhov, A., Osipov, S., Ahmadov, R., Grell, G., Cady-Pereira, K., et al. (2021). How does a  
686 Pinatubo-size volcanic cloud reach the middle stratosphere? *Journal of Geophysical Research:*  
687 *Atmospheres*, 126, e2020JD033829. <https://doi.org/10.1029/2020JD033829>

688 Tackett, J. L., Winker, D. M., Getzewich, B. J., Vaughan, M. A., Young, S. A., and Kar, J.: CALIPSO lidar level 3  
689 aerosol profile product: version 3 algorithm design, *Atmos. Meas. Tech.*, 11, 4129–  
690 4152, <https://doi.org/10.5194/amt-11-4129-2018>, 2018.

691 Theys, N., Campion, R., Clarisse, L., Brenot, H., van Gent, J., Dils, B., Corradini, S., Merucci, L., Coheur, P.-F.,  
692 Van Roozendael, M., Hurtmans, D., Clerbaux, C., Tait, S., & Ferrucci, F. (2013). Volcanic SO<sub>2</sub> fluxes  
693 derived from satellite data: a survey using OMI, GOME-2, IASI and MODIS. *Atmospheric Chemistry and*  
694 *Physics*, 13(12), 5945–5968. <https://doi.org/10.5194/acp-13-5945-2013>  
695

696 Theys, N., De Smedt, I., Yu, H., Danckaert, T., van Gent, J., Hörmann, C., Wagner, T., Hedelt, P., Bauer, H.,  
697 Romahn, F., Pedergnana, M., Loyola, D., & Van Roozendael, M. (2017). Sulfur dioxide retrievals from  
698 TROPOMI onboard Sentinel-5 Precursor: algorithm theoretical basis. *Atmospheric Measurement*  
699 *Techniques*, 10(1), 119–153. <https://doi.org/10.5194/amt-10-119-2017>  
700

701 Theys, N., Fioletov, V., Li, C., De Smedt, I., Lerot, C., McLinden, C., Krotkov, N., Griffin, D., Clarisse, L., Hedelt,  
702 P., Loyola, D., Wagner, T., Kumar, V., Innes, A., Ribas, R., Hendrick, F., Vlietinck, J., Brenot, H., & Van  
703 Roozendael, M. (2021). A sulfur dioxide Covariance-Based Retrieval Algorithm (COBRA): application to  
704 TROPOMI reveals new emission sources. *Atmospheric Chemistry and Physics*, 21(22), 16727–16744.  
705 <https://doi.org/10.5194/acp-21-16727-2021>  
706

707 Theys, N., Lerot, C., Brenot, H., van Gent, J., De Smedt, I., Clarisse, L., Burton, M., Varnam, M., Hayer, C., Esse,

708 B., & Van Roozendaal, M. (2022). Improved retrieval of SO<sub>2</sub> plume height from TROPOMI using an  
709 iterative Covariance-Based Retrieval Algorithm. *Atmospheric Measurement Techniques*, 15(16), 4801–  
710 4817. <https://doi.org/10.5194/amt-15-4801-2022>  
711  
712  
713 Tournigand, P.-Y., Cigala, V., Lasota, E., Hammouti, M., Clarisse, L., Brenot, H., Prata, F., Kirchengast, G.,  
714 Steiner, A. K., & Biondi, R. (2020). A multi-sensor satellite-based archive of the largest SO<sub>2</sub> volcanic  
715 eruptions since 2006. *Earth System Science Data*, 12(4), 3139–3159. [https://doi.org/10.5194/essd-12-3139-](https://doi.org/10.5194/essd-12-3139-2020)  
716 2020  
717  
718 Vaughan, G., Wareing, D., and Ricketts, H.: Measurement Report: Lidar measurements of stratospheric aerosol  
719 following the 2019 Raikoke and Ulawun volcanic eruptions, *Atmos. Chem. Phys.*, 21, 5597–5604,  
720 <https://doi.org/10.5194/acp-21-5597-2021>, 2021.  
721  
722 Veefkind, J. P., Aben, I., McMullan, K., Förster, H., de Vries, J., Otter, G., Claas, J., Eskes, H. J., de Haan, J. F.,  
723 Kleipool, Q., van Weele, M., Hasekamp, O., Hoogeveen, R., Landgraf, J., Snel, R., Tol, P., Ingmann, P.,  
724 Voors, R., Kruizinga, B., ... Levelt, P. F. (2012). TROPOMI on the ESA Sentinel-5 Precursor: A GMES  
725 mission for global observations of the atmospheric composition for climate, air quality and ozone layer  
726 applications. *Remote Sensing of Environment*, 120, 70–83.  
727 <https://doi.org/https://doi.org/10.1016/j.rse.2011.09.027>  
728  
729 Vernier, J.-P., Fairlie, T. D., Deshler, T., Natarajan, M., Knepp, T., Foster, K., Wienhold, F. G., Bedka, K. M.,  
730 Thomason, L., & Trepte, C. (2016). In situ and space-based observations of the Kelud volcanic plume: The  
731 persistence of ash in the lower stratosphere. *Journal of Geophysical Research*, 121(18).  
732 <https://doi.org/10.1002/2016JD025344>  
733  
734 Vernier, J.-P., Fairlie, T. D., Murray, J. J., Tupper, A., Trepte, C., Winker, D., Pelon, J., Garnier, A., Jumelet, J.,  
735 Pavolonis, M., Omar, A. H., & Powell, K. A. (2013). An advanced system to monitor the 3D structure of  
736 diffuse volcanic ash clouds. *Journal of Applied Meteorology and Climatology*, 52(9).  
737 <https://doi.org/10.1175/JAMC-D-12-0279.1>  
738  
739 Vömel H, Evan S, Tully M. Water vapor injection into the stratosphere by Hunga Tonga-Hunga Ha'apai. *Science*.  
740 2022 Sep 23;377(6613):1444-1447. doi: 10.1126/science.abq2299. Epub 2022 Sep 22. PMID: 36137033.  
741  
742 Winker, D. M., Tackett, J. L., Getzewich, B. J., Liu, Z., Vaughan, M. A., & Rogers, R. R. (2013). The global 3-D  
743 distribution of tropospheric aerosols as characterized by CALIOP. *Atmospheric Chemistry and Physics*, 13(6),  
744 3345–3361. <https://doi.org/10.5194/acp-13-3345-2013>

745 Winker, D. M., Pelon, J., Coakley, J. A., Ackerman, S. A., Charlson, R. J., Colarco, P. R., Flamant, P., Fu, Q., Hoff,  
746 R. M., Kittaka, C., Kubar, T. L., Le Treut, H., McCormick, M. P., Mégie, G., Poole, L., Powell, K., Treppe,  
747 C., Vaughan, M. A., & Wielicki, B. A. (2010). The CALIPSO Mission. *Bulletin of the American*  
748 *Meteorological Society*, 91(9), 1211–1230. <https://doi.org/10.1175/2010BAMS3009.1>

749 Wrana, F., Niemeier, U., Thomason, L. W., Wallis, S., and von Savigny, C.: Stratospheric aerosol size reduction  
750 after volcanic eruptions, *Atmos. Chem. Phys.*, 23, 9725–9743, <https://doi.org/10.5194/acp-23-9725-2023>,  
751 2023.

752 Zängl, G., Reinert, D., Rípodas, P., and Baldauf, M.: The ICON (ICOsahedral Non-hydrostatic) modelling  
753 framework of DWD and MPI-M: Description of the non-hydrostatic dynamical core, *Q. J. Roy. Meteor.*  
754 *Soc.*, 141, 563–579, <https://doi.org/10.1002/qj.2378>, 2015. a, b, c

755

756 Zhu, Y., Toon, O.B., Jensen, E.J. et al. Persisting volcanic ash particles impact stratospheric SO<sub>2</sub> lifetime and  
757 aerosol optical properties. *Nat Commun* 11, 4526 (2020). <https://doi.org/10.1038/s41467-020-18352-5>  
758

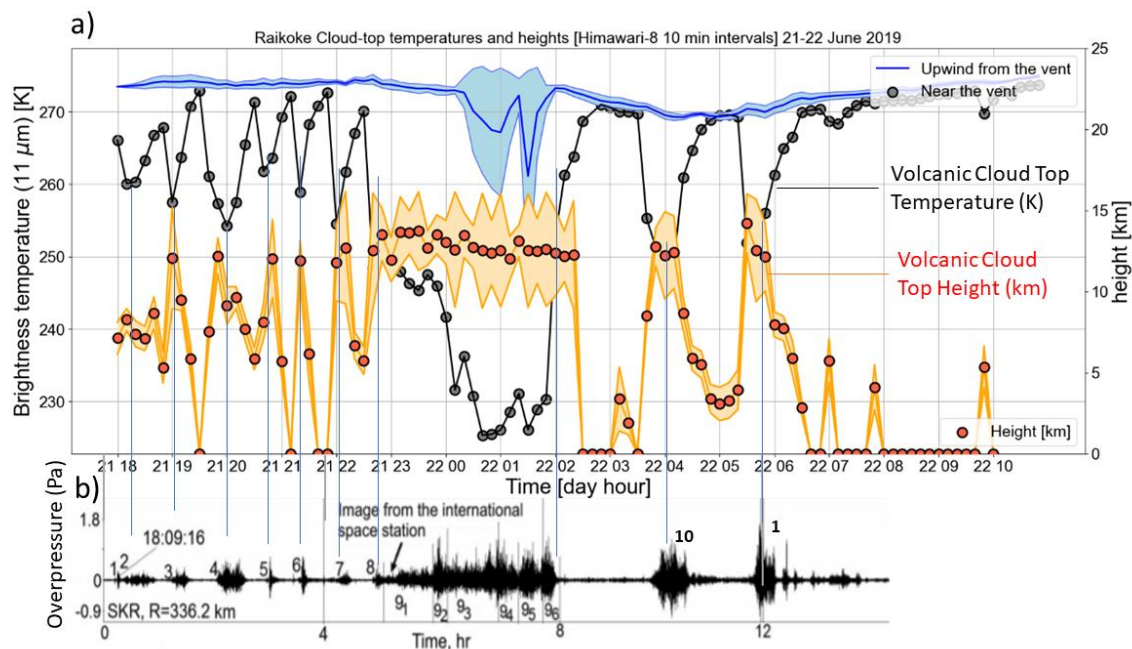
759

760

761 **Figures.**

762

763

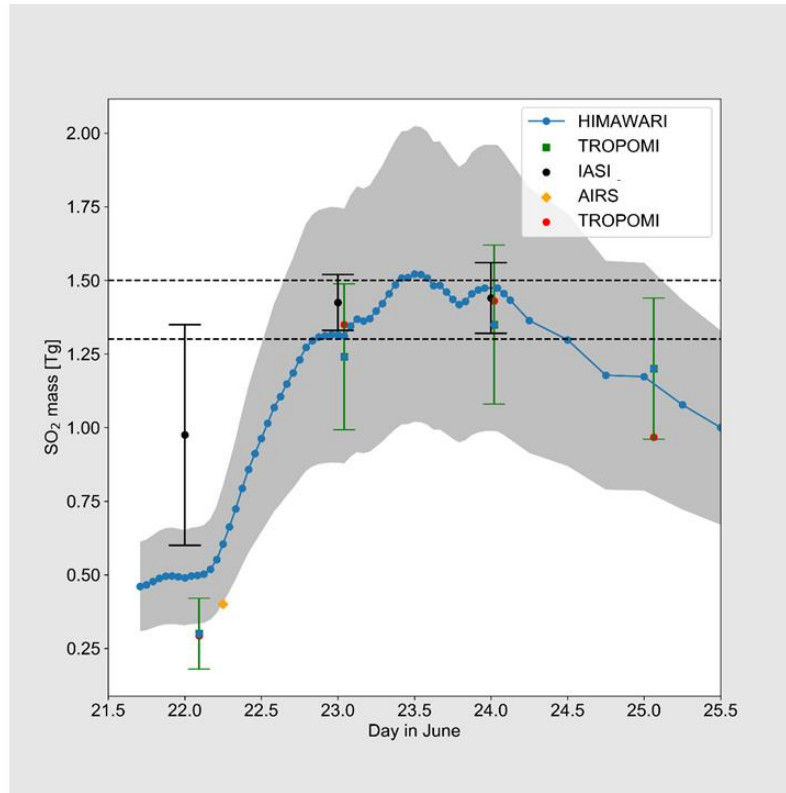


764

765 **Figure 1. (Top)**Time series of Himawari-8 cloud-top brightness temperatures from the 11 micron  
766 channel. The blue line corresponds to the mean of 3x3 pixels at a point upwind, but close to, the vent. The  
767 shaded region represents  $\pm 1$  sigma from the mean. The grey dots are brightness temperatures at the pixel  
768 closest to the vent. The brightness temperature (BT) rapid decreases at the vent, that are not coincident with  
769 the upwind values, suggest eruptive columns with cold, high cloud tops. The BT values should be read from  
770 the left-hand ordinate axis. The orange dots with uncertainties (shaded) correspond to cloud-top heights  
771 (right-hand ordinate axis) taken from Prata et al. (2022) (Bottom) Modified from Fig.7 from (Firstov et al.,  
772 2020) showing InfraSound (IS) signals (overpressure) during the first 12h after the beginning of the Raikoke  
773 eruption which started near 17:53:54 UTC on June 21 2019 from a ground station on Paramushir Island  
774 (SKR, southern tip of Kamchatka). The numbers indicate the separate episodes of the eruption, defined by  
775 the records at SKR. The blue lines connect those IS episodes with observed minimum in cloud top  
776 temperature. R corresponds to the distance between the station and the Raikoke volcano.

777

778



779

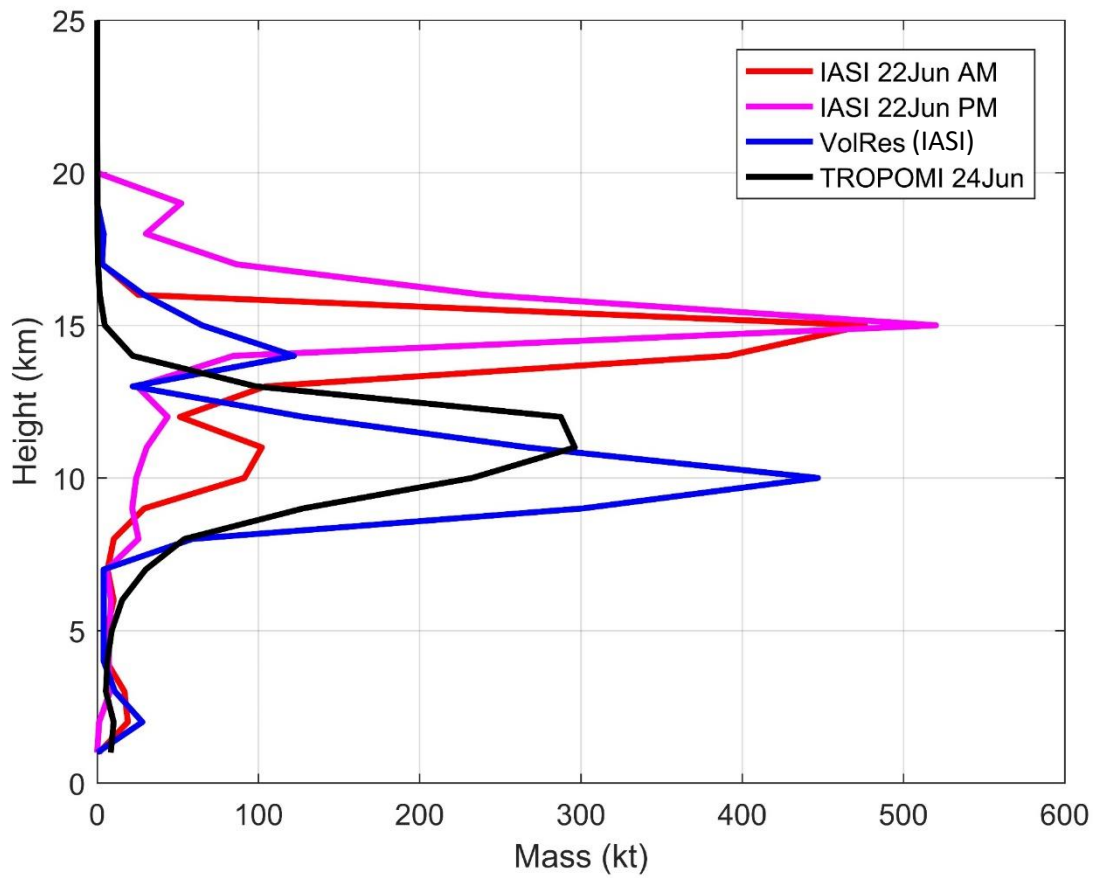
780 **Figure 2. Total SO<sub>2</sub> mass (Tg) as a function of time in June 2019 estimated from various satellite sensors for**  
 781 **the eruption of Raikoke. The grey-colored region indicates the uncertainty range of the Himawari-8 (AHI)**  
 782 **retrievals. A ±20% uncertainty has been placed on the TROPOMI estimates. The IASI estimates come from**  
 783 **different satellites and times of day (day/night); the vertical lines on these data indicate the range of the**  
 784 **estimations. Himawari-8 samples every 10 minutes. After 24 June retrievals were performed at longer**  
 785 **intervals. Distributed to VolRes on 06/28/2019.**

786

787

788





789

790 **Figure 3: SO<sub>2</sub> mass altitude distribution from IASI (refined analysis), VolRes (IASI initial estimate) and**  
 791 **TROPOMI. The associated data is provided in Table 2.**

792

793

794

795

796

797

798

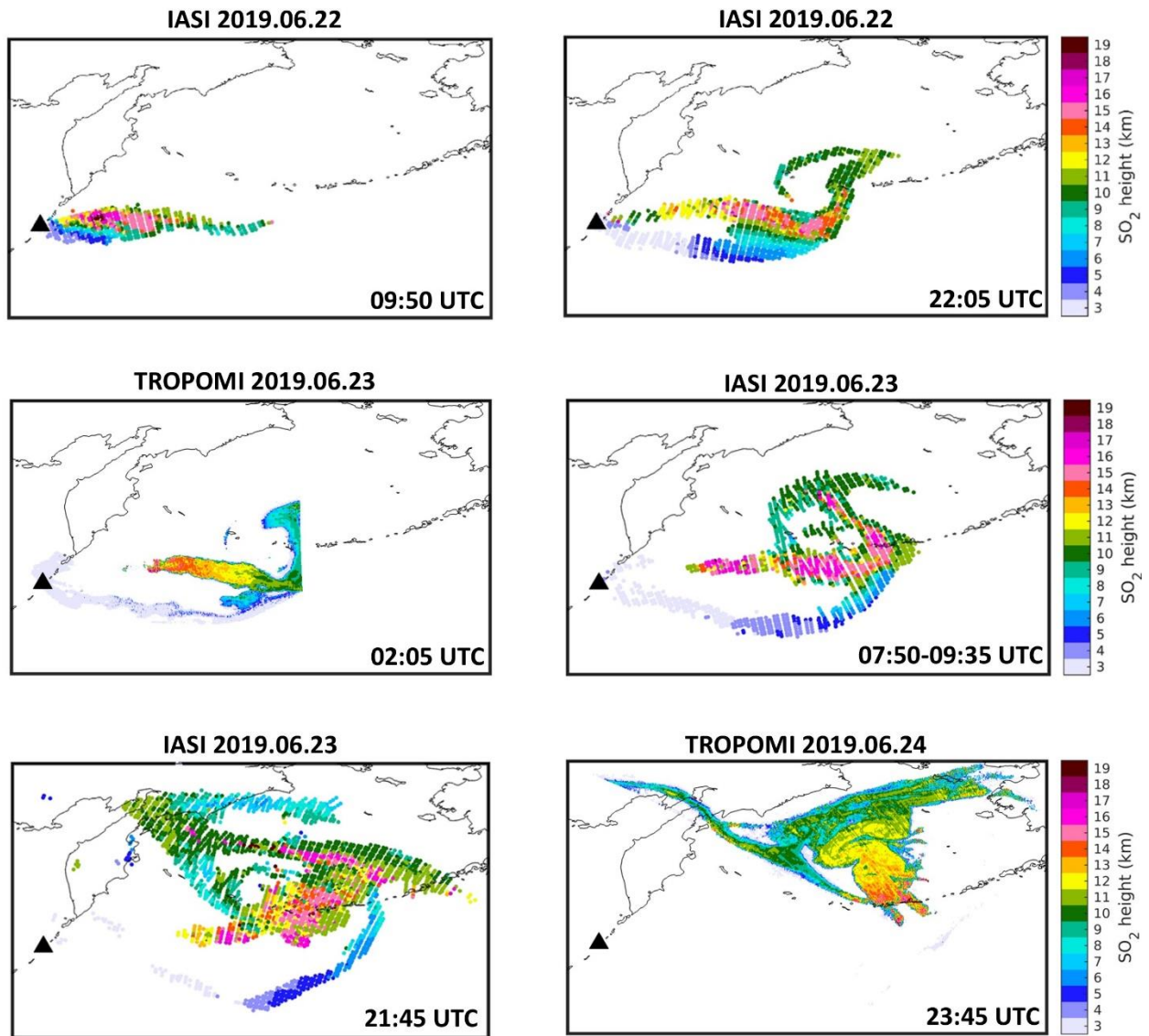
799

800

801

802

803



804

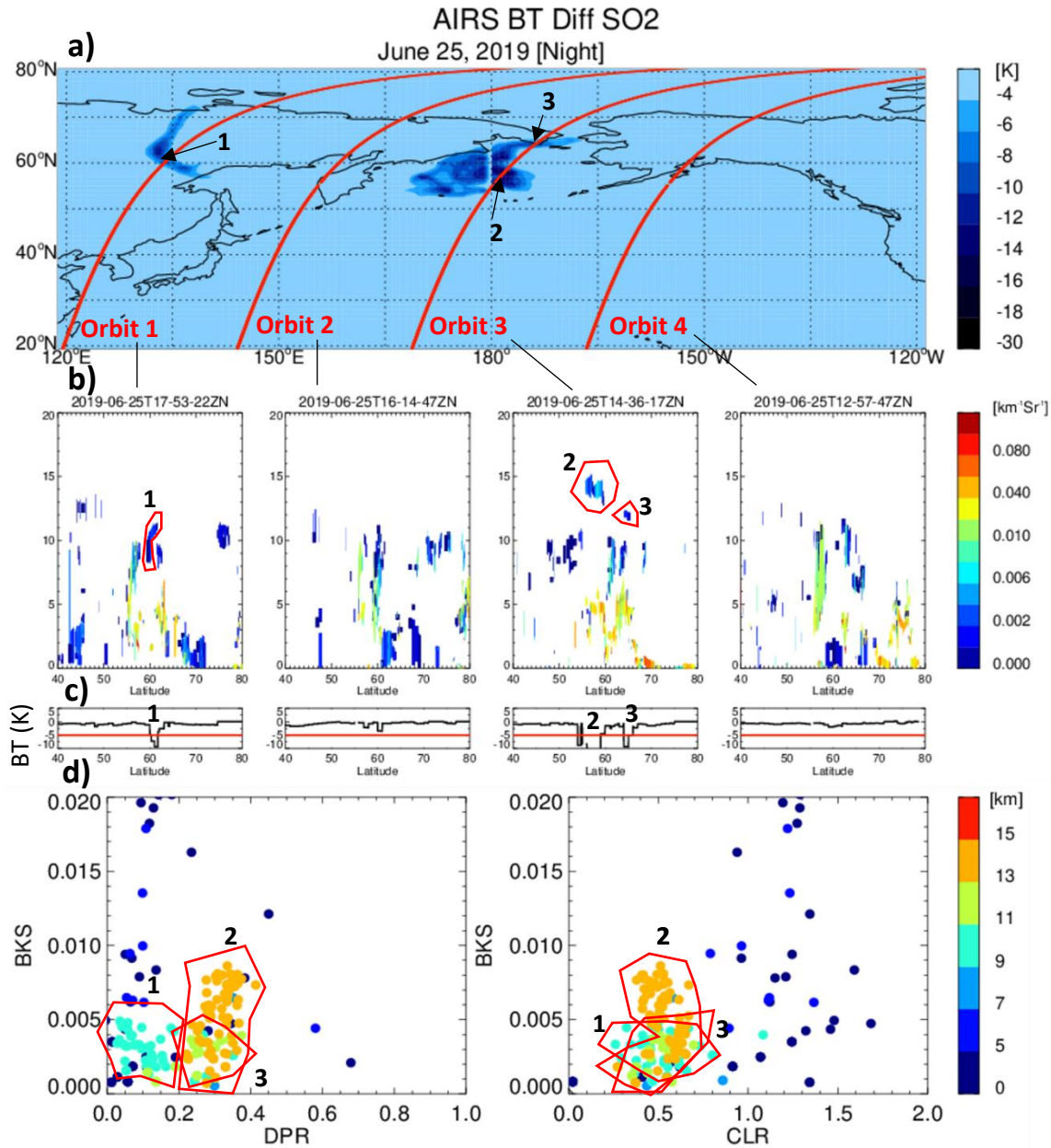
805 **Figure 4: Examples of SO<sub>2</sub> height retrievals from IASI (refined analysis) and TROPOMI for Raikoke eruption**  
806 **for 22-24 June 2019. The Raikoke volcano is marked by a black triangle. Approximate overpass times are**  
807 **indicated in each panel.**

808

809

810

811



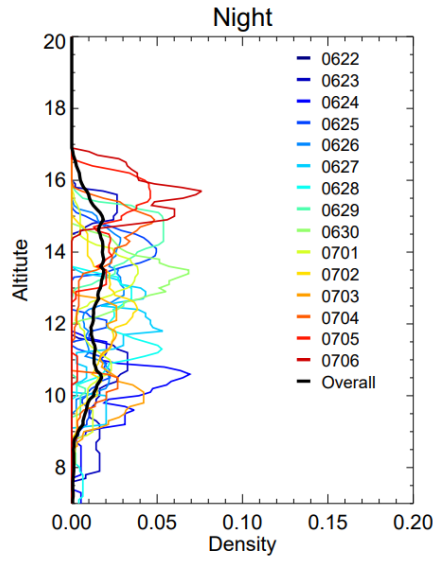
812

813 **Figure 5. (a) AIRS Nighttime Brightness Temperature Difference (BTD) ( $1361.44\text{-}1433.06\text{ cm}^{-1}$ ) on 25 June**  
 814 **2022 together with 4 CALIOP ground-tracks (red). (b) Corresponding aerosol and cloud layer products from**  
 815 **CALIOP level 2V4.2 product and (c) extracted AIRS BTD extracted along the CALIOP orbit tracks. The red**  
 816 **line correspond to the threshold used for detecting volcanic enhancement (d) diagrams of particular**  
 817 **backscatter (BKS) as a function of mean layer particulate DePolarization Ratio (DPR) (left) and particulate**  
 818 **CoLor Ratio (CLR) (right) derived from CALIOP and colored by mid-layer altitudes.**

819

820

821



822

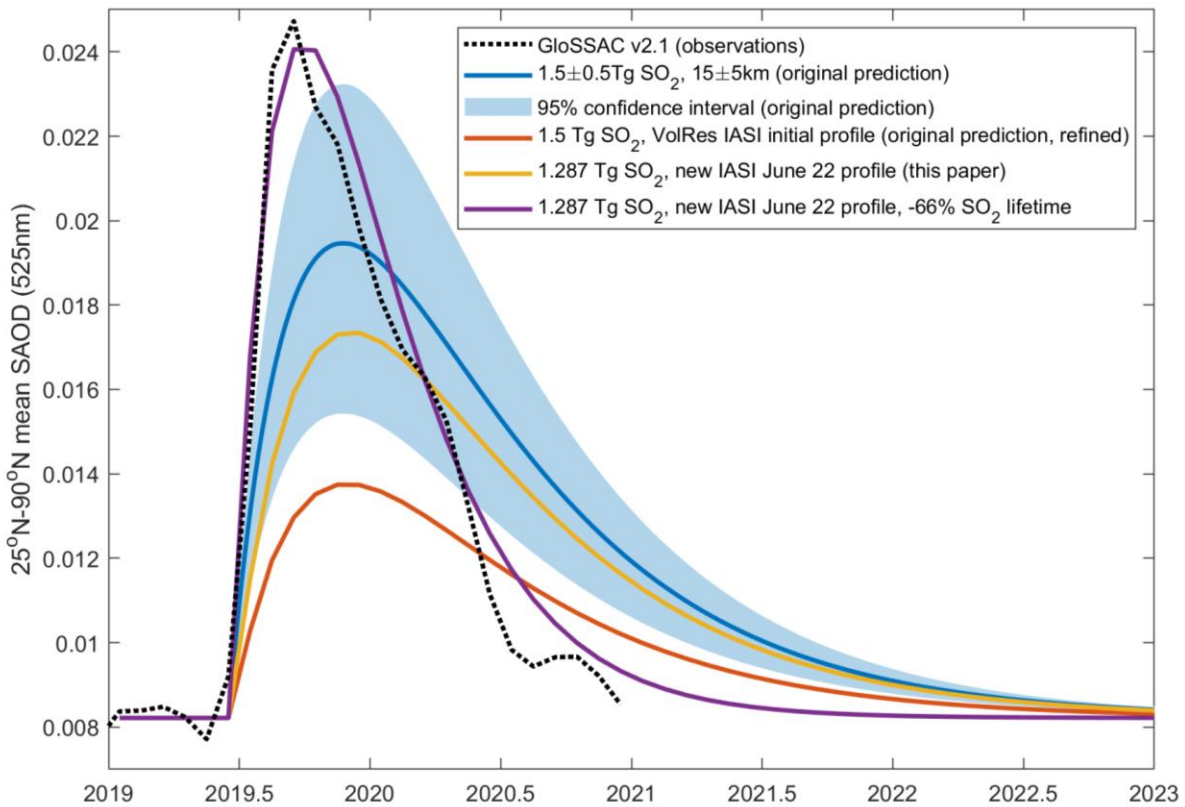
823 **Figure 6. Daily nighttime Probability Density Function profiles of the mid-layer geometric altitude for volcanic**  
 824 **layers observed by CALIOP/AIRS using plume identification criterion when  $DPR < 0.4$  and  $CLR < 0.7$  and**  
 825 **altitude  $> 5\text{km}$  and  $BTD < -6\text{K}$  between 06/22 and 07/06. The black line is the overall pdf profile using all**  
 826 **nighttime data between 06/22 and 07/06.**

827

828

829

830



831

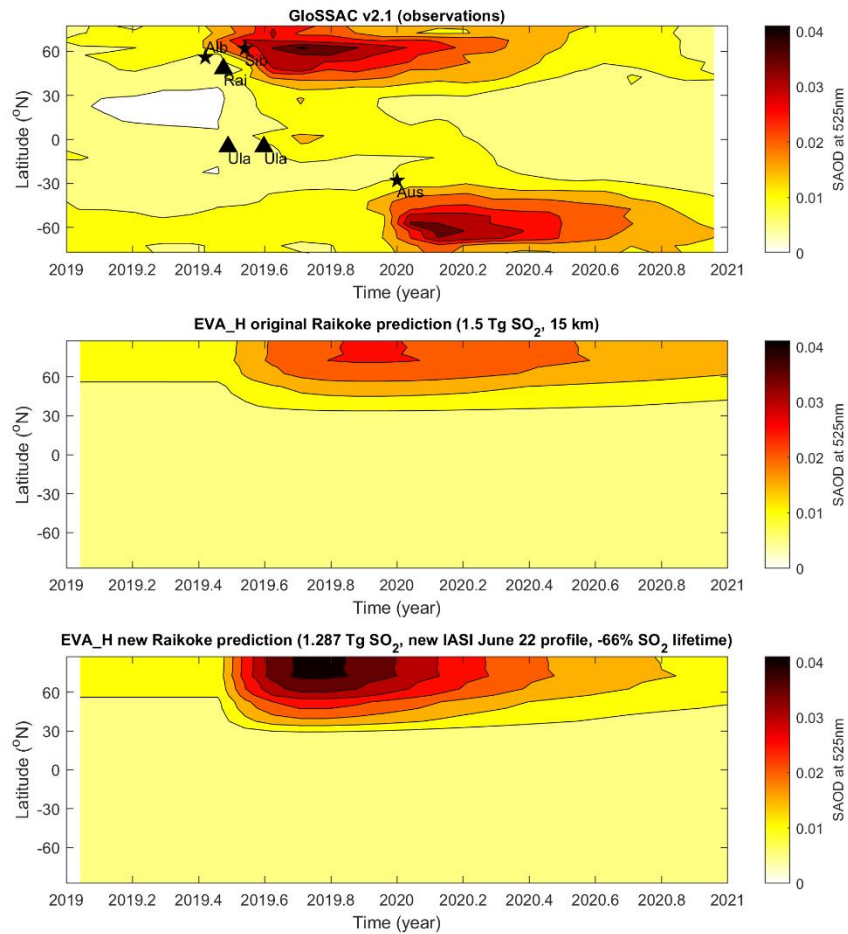
832 **Figure 7: Northern Hemisphere (25°N-90°N) monthly-mean SAOD at 525nm as projected by EVA\_H**  
 833 **(continuous colored lines) and observed (GloSSAC v2.1, black dashed line). The light blue shading and line**  
 834 **shows the first projection made at the time of the eruption and its confidence interval based on an injection**  
 835 **height of 15+/-5km and SO<sub>2</sub> mass of 1.5+/-0.5 Tg. The orange line shows the second projection made at the**  
 836 **time of the eruption using the VolRes IASI initial profile. The yellow line shows a new projection using the**  
 837 **new VolRes IASI June 22 profile presented in this study (Figure 3). The violet line uses the same profile, but**  
 838 **the SO<sub>2</sub>-to-aerosol conversion timescale in EVA\_H reduced by 66%.**

839

840

841

842



843

844 **Figure 8: SAOD at 525nm as observed (GloSSAC v2.1, top) and projected by EVA\_H following the Raikoke**  
 845 **2019 eruption (middle) and using the revised IASI June 22 SO<sub>2</sub> profile presented in this paper along with the**  
 846 **adjusted (-66%) SO<sub>2</sub>-to-aerosol conversion timescale in EVA\_H (bottom). EVA\_H was run only with the**  
 847 **Raikoke injections, and not with injections associated with the Ulawun 2019 eruptions (denoted by black**  
 848 **triangles in the top panel) nor with wildfire events in Alberta, Siberia (2019) and Australia (2020) (denoted by**  
 849 **black stars in the top panel).**

850

851

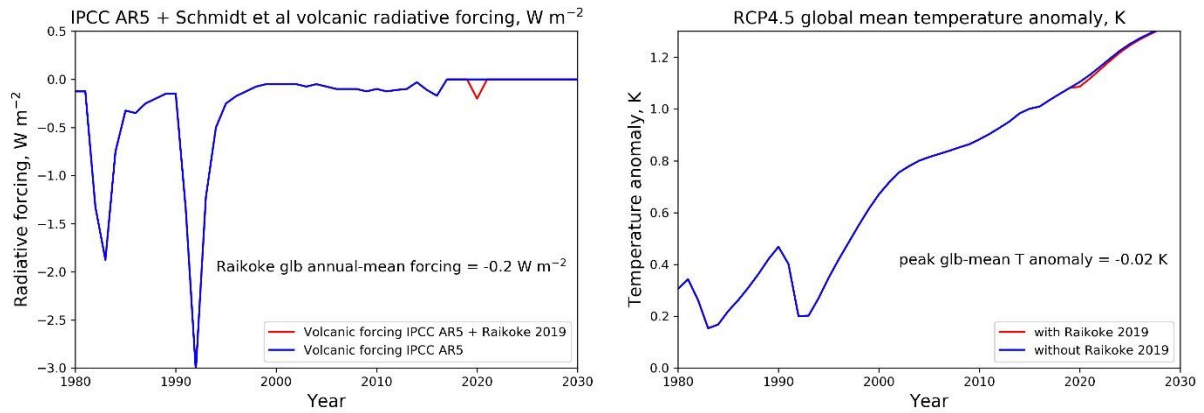
852

853

854

855

856



857

858 **Figure 9: Annual global mean volcanic radiative forcing (left) and corresponding annual global mean surface**  
 859 **temperature anomaly calculated using the climate response model FaIR (Smith et al., 2018) (right). Blue and**  
 860 **red lines show results with and without accounting for the 2019 Raikoke eruption, respectively. This is the**  
 861 **original figure shared on the VolRes mailing list on 06/26/19.**

862

863

864

865

866

867

868

869

870

871

872

873

874

875

876

877

878

879

880

Date	Data type	Activities	Data variables	Platform	Add. Information
06/24	Satellite	SO2 and plume height maps 06/24 & 06/25	SO2 total column (DU) and concentration (ppmv ?)	TROPOMI/Sentinel 5P	Polar Orbit/ESA
06/24	Satellite	Aerosol maps and profiles when ?	Aerosol extinction (km-1)	NPP/OMPS	Polar Orbit/NASA
06/25	Satellite	SO2 maps 06/21 & 06/22	SO2 total column (DU)	Metop/IASI	Polar Orbit/Eumetsat
06/25	Satellite	Ash and SO2 total column	Ash signature (11-12 um) and SO2 UTLS (VCD DU)	AHI/HIMAWARI-8	Geo Orbit/JAXA
06/25	Satellite	Plume heights and optical properties	Backscatter and depolarization at 532 and 1064 nm	CALIOP/CALIPSO	Polar Orbit/NASA
06/25	Satellite	Maps of plume height and properties 06/23	Height (km) and AOD, angstrom coeff, SSA	MISR/Terra	Polar Orbit/NASA
06/25	Model	Volcanic plume maps at 100 and 140 hPa	Aerosol extinction at XX nm	WACCM	Model type
06/25	Model	Impacts on stratospheric aerosol	Stratospheric AOD	GEOS-5	
06/26	Satellite	Mass distribution profile on 06/23	Mass per levels (kt)	TROPOMI/Sentinel 5P	Polar Orbit/ESA
06/26	Satellite	SO2 plume vertical information	SO2 mixing ratio (ppbv)	MLS/Aura	Polar Orbit/ESA
06/26	Model	Radiative and climate impacts	RF TOA (w/m2)	??	
06/28	Model	Trajectory simulation of Raikoke dispersion	Plume height (km)	Langley Trajectory Model	GEOS-5 wind data
07/03	Satellite	Plume height and properties	Backscatter and depolarization at 532 and 1064 nm	CALIOP/CALIPSO	Polar Orbit/ESA
07/09	Model	SO2 and ash plume dispersion 06/21 to 06/25	Ash and SO2 mass concentration	ICONN-ART	
07/10	Ground-based lidar	Vertical plume profiles 07/05	Scattering ratio at 532 nm	OHP/LTA	
07/10	Satellite	Plume height and properties	Backscatter and depolarization at 532 and 1064 nm	CALIOP/CALIPSO	Polar Orbit/NASA
07/10	Satellite	Latitudinal time series	Aerosol extinction (km-1)	NPP/OMPS	NASA
07/16	Satellite	Animation of aerosol maps at 12.5 km, 13.5 km, 14.5 km and 16.5 km across the NH. 06/11 to 07/14	Aerosol extinction (km-1)	OMPS/NPP	Polar Orbit/NASA
07/17	Ground-based lidar	Volcanic aerosol profiles 06/29 and 07/08	RSC 1064 nm	SIRTA	
07/19	Satellite	Maps of SO2 centered in Indonesia/Australia (from 06/26 to 07/12), Ulawun eruption	SO2 DU	TROPOMI/Sentinel 5P	Polar Orbit/ESA
07/20	Satellite	Animation of aerosol maps at 18.5 km from 06/27 to 07/17	Aerosol extinction (km-1) at 674 nm	OMPS/NPP	Polar Orbit/NASA
07/21	Ground-based lidar	Volcanic aerosol profiles on 07/18 and 07/20	Scattering Ratio at 532 nm	OHP LTA	
08/07	Satellite	Animation of aerosol maps at 20.5 km	Aerosol extinction (km-1) at 674 nm	OMPS/NPP	Polar Orbit/NASA
08/24	Satellite	Volcanic plumes cross-section 11-20 Aug 2019	Scattering Ratio at 532 nm	CALIOP/CALIPSO	Polar Orbit/NASA
09/04	Balloon	Aerosol concentration profiles on 08/26 in Wyoming	Aerosol concentration for $r > 0.005 \mu m, 0.092, 0.15, 0.28$	Balloon	WOPC
09/17	Ground-	Atmospheric profiles of aerosols and	Backscatter profiles at 532 nm	Lidar LOA	

881

882

883 **Table 1: VolRes activities during the first 2 months after the Raikoke eruption.**



884

Altitude (km)	VolRes IASI initial profile	IASI 22 June 2019 (AM)	IASI 22 June 2019 (PM)	TROPOMI 24 June 2019
1	0	1.1	0	8.4
2	28	19.0	1.2	10.2
3	11	16.9	8	5.4
4	4	5.6	7.1	6.3
5	4	6.0	7.9	9.0
6	4	10.2	8.5	15.5
7	4	6.4	6.0	30.1
8	59	10.3	25.6	54.1
9	301	29.2	21.7	127.6
10	446	91.3	24.2	232.6
11	266	102.1	30.7	296.2
12	128	51.3	43.7	287.5
13	22	104.4	24.8	98.4
14	122	390.9	84.5	22.0
15	65	476.2	520.2	4.7
16	29	25.5	239.7	1.63
17	3	3.3	86.4	0.53
18	4	2.6	30.2	0.19
19	0	0	52.1	0.14
20	0	0	0	0.1
<b>Total</b>	<b>1500 kt (scaled)</b>	<b>1352.3 kt</b>	<b>1222.5 kt</b>	<b>1210.6 kt</b>

885

886 **Table 2: SO<sub>2</sub> mass profile (in kt) derived from IASI and TROPOMI for the Raikoke eruption.**

887

888